3-1-2020

Basal forebrain volume reliably predicts the cortical spread of Alzheimer's degeneration

Sara Fernández-Cabello
Universitat Salzburg

Martin Kronbichler
Universitat Salzburg

Koene R.A. van Dijk
Pfizer Inc.

James A. Goodman
Pfizer Inc.

R. Nathan Spreng
Institut-Hôpital Neurologique de Montréal

See next page for additional authors

doi:10.1093/brain/awaa012 BRAIN 2020: 143; 993–1009 | 993

BRAIN
A JOURNAL OF NEUROLOGY

Basal forebrain volume reliably predicts the cortical spread of Alzheimer's degeneration

Sara Fernández-Cabello,[1,2] Martin Kronbichler,[1,2,3] Koene R.A. Van Dijk,[4] James A. Goodman,[4] R. Nathan Spreng [5,6,7,8] and Taylor W. Schmitz[9,10] on behalf of the Alzheimer's Disease Neuroimaging Initiative*

*Data used in preparation of this article were obtained from the Alzheimer's Disease Neuroimaging Initiative (ADNI) database (adni.loni.usc.edu). As such, the investigators within the ADNI contributed to the design and implementation of ADNI and/or provided data but did not participate in analysis or writing of this report. A complete listing of ADNI investigators can be found at: http://adni.loni.usc.edu/wp-content/uploads/how_to_apply/ADNI_Acknowledgement_List.pdf

Alzheimer's disease neurodegeneration is thought to spread across anatomically and functionally connected brain regions. However, the precise sequence of spread remains ambiguous. The prevailing model used to guide *in vivo* human neuroimaging and non-human animal research assumes that Alzheimer's degeneration starts in the entorhinal cortices, before spreading to the temporoparietal cortex. Challenging this model, we previously provided evidence that *in vivo* markers of neurodegeneration within the nucleus basalis of Meynert (NbM), a subregion of the basal forebrain heavily populated by cortically projecting cholinergic neurons, precedes and predicts entorhinal degeneration. There have been few systematic attempts at directly comparing staging models using *in vivo* longitudinal biomarker data, and none to our knowledge testing if comparative evidence generalizes across independent samples. Here we addressed the sequence of pathological staging in Alzheimer's disease using two independent samples of the Alzheimer's Disease Neuroimaging Initiative ($n1 = 284$; $n2 = 553$) with harmonized CSF assays of amyloid-β and hyperphosphorylated tau (pTau), and longitudinal structural MRI data over 2 years. We derived measures of grey matter degeneration in *a priori* NbM and the entorhinal cortical regions of interest. To examine the spreading of degeneration, we used a predictive modelling strategy that tests whether baseline grey matter volume in a seed region accounts for longitudinal change in a target region. We demonstrated that predictive spread favoured the NbM→entorhinal over the entorhinal→NbM model. This evidence generalized across the independent samples. We also showed that CSF concentrations of pTau/amyloid-β moderated the observed predictive relationship, consistent with evidence in rodent models of an underlying trans-synaptic mechanism of pathophysiological spread. The moderating effect of CSF was robust to additional factors, including clinical diagnosis. We then applied our predictive modelling strategy to an exploratory whole-brain voxel-wise analysis to examine the spatial specificity of the NbM→entorhinal model. We found that smaller baseline NbM volumes predicted greater degeneration in localized regions of the entorhinal and perirhinal cortices. By contrast, smaller baseline entorhinal volumes predicted degeneration in the medial temporal cortex, recapitulating a prior influential staging model. Our findings suggest that degeneration of the basal forebrain cholinergic projection system is a robust and reliable upstream event of entorhinal and neocortical degeneration, calling into question a prevailing view of Alzheimer's disease pathogenesis.

1 Department of Psychology, University of Salzburg, Salzburg, Austria
2 Centre for Cognitive Neuroscience, University of Salzburg, Salzburg, Austria
3 Neuroscience Institute, Christian-Doppler Medical Centre, Paracelsus Medical University, Salzburg, Austria
4 Clinical and Translational Imaging, Early Clinical Development, Pfizer Inc, Cambridge, MA, USA
5 Laboratory of Brain and Cognition, Montreal Neurological Institute, Department of Neurology and Neurosurgery, McGill University, Montreal, QC, Canada
6 Departments of Psychiatry and Psychology, McGill University, Montreal, QC, Canada

Received June 21, 2019. Revised November 21, 2019. Accepted December 4, 2019.

7 Douglas Mental Health University Institute, Verdun, QC, Canada
8 McConnell Brain Imaging Centre, McGill University, Montreal, QC, Canada
9 Brain and Mind Institute, Western University, London, ON, Canada
10 Department of Physiology and Pharmacology, Western University, London, ON, Canada

Keywords: Alzheimer's disease; basal forebrain; NbM; entorhinal cortex; nucleus basalis of Meynert

Abbreviations: ADNI = Alzheimer's Disease Neuroimaging Initiative; APC = annual per cent change; EC = entorhinal cortex; NbM = nucleus basalis of Meynert; pTau = hyperphosphorylated tau

Introduction

Alzheimer's disease neuropathology progresses in stages, with certain brain regions affected by neuronal accumulation of insoluble amyloid-β and hyperphosphorylated tau (pTau) before others. The preferential accumulation of amyloid-β and pTau in certain brain regions may reflect the selective vulnerabilities of local neuronal populations to these age-related 'proteinopathies' (Davies and Maloney, 1976; Whitehouse *et al.*, 1981; Arendt *et al.*, 1985, 2015; Mesulam *et al.*, 2004; Mattson and Magnus, 2006; Geula *et al.*, 2008; Braak and Del Tredici, 2011, 2015; Braak *et al.*, 2011; Saxena and Caroni, 2011; Baker-Nigh *et al.*, 2015; Hanna Al-Shaikh *et al.*, 2019), which then spread to targets of the vulnerable population's projection system (Warren *et al.*, 2013). Evidence in both mouse models of Alzheimer's disease (de Calignon *et al.*, 2012; Liu *et al.*, 2012; Khan *et al.*, 2014; Wu *et al.*, 2016) and in human Alzheimer's disease patients (Grothe *et al.*, 2018; Sepulcre *et al.*, 2018; Hanseeuw *et al.*, 2019) indicates that accumulated amyloid-β and pTau spreads across anatomically and functionally connected brain regions over time. Despite these observations, it remains ambiguous how the accumulation of amyloid-β and pTau relates to the spread of structural neurodegeneration across brain regions over time (Harrison *et al.*, 2019). This question can only be resolved by integrating sensitive biomarkers of amyloid-β and pTau with *in vivo* longitudinal measures of microstructural degeneration in both the subcortical and cortical brain areas.

Post-mortem histology studies have linked abnormal amyloid-β and pTau accumulation to early neurodegeneration in the entorhinal cortex and in the nucleus basalis of Meynert (NbM)—also referred to as Ch4/Ch4p (Mesulam *et al.*, 1983*a*, *b*; Mesulam and Geula, 1988)—the largest of the cholinergic cell clusters constituting the basal forebrain (Davies and Maloney, 1976; Whitehouse *et al.*, 1981; Arendt *et al.*, 1985, 2015; Mesulam *et al.*, 2004; Geula *et al.*, 2008; Baker-Nigh *et al.*, 2015; Braak and Del Tredici, 2015; Hanna Al-Shaikh *et al.*, 2019). The selective vulnerability of neurons in the entorhinal cortex and NbM to these proteinopathies is attributed to their enormous size and complexity of their axonal projections, and the high propensity for sustained plasticity in these projections in adulthood (Mesulam, 1999; Mattson and Magnus, 2006; Saxena and Caroni, 2011; Wu *et al.*, 2014; Roussarie *et al.*, 2019). One individual spiny stellate neuron in layer II of the entorhinal cortex innervates the entire transverse axis of the dentate gyrus, CA2/CA3 and the subiculum (Tamamaki and Nojyo, 1993). Cholinergic neurons also have extremely long and complex branching with the full arborization length of a single neuron estimated in humans to be >100 m (Wu *et al.*, 2014). Unlike age-resilient neurons in the primary sensory cortices, both entorhinal cortex layer II glutamatergic neurons and NbM cholinergic neurons must continually remodel their axonal arborizations and synapses throughout the adult lifespan due to their central role in attention and memory (Sarter *et al.*, 2003; Hasselmo, 2006; Botly and De Rosa, 2009; Heys *et al.*, 2010; Gu and Yakel, 2011; Mitsushima *et al.*, 2013; Schmitz and Duncan, 2018).

Although since the 1970s human post-mortem histology research has provided consistent evidence for a subcortical phase of Alzheimer's disease pathology that precedes and predicts cortical degeneration (Davies and Maloney, 1976; Whitehouse *et al.*, 1981; Arendt *et al.*, 1985, 2015; Mesulam *et al.*, 2004; Geula *et al.*, 2008; Braak and Del Tredici, 2011, 2015; Braak *et al.*, 2011; Baker-Nigh *et al.*, 2015; Hanna Al-Shaikh *et al.*, 2019), the prevailing Alzheimer's staging model used to guide *in vivo* neuroimaging research in both humans and rodents assumes an entorhinal cortex origin. Structural MRI studies in humans tend to focus on the progression of abnormal grey matter loss in entorhinal cortex and hippocampal targets of its projections (de Toledo-Morrell *et al.*, 2000, 2004; Dickerson *et al.*, 2001; Du *et al.*, 2001; Good *et al.*, 2002; Karas *et al.*, 2004; Hirata *et al.*, 2005; Kloppel *et al.*, 2008; Gerardin *et al.*, 2009; Frisoni *et al.*, 2010; Sorensen *et al.*, 2016; Hett *et al.*, 2019). Yet these studies frequently exclude subcortical regions such as the NbM from analysis entirely. Similarly, cross-species translational research using mouse models of Alzheimer's disease tend to assume an entorhinal cortex origin. Examples include recent influential work showing that accumulated amyloid pathology in entorhinal cortex neurons potentiates hyperphosphorylation of tau proteins, which then spread via trans-synaptic mechanisms to distal neocortical targets of entorhinal cortex, including the medial temporal and posterior parietal cortex (de Calignon *et al.*, 2012; Liu *et al.*, 2012; Khan *et al.*, 2014; Wu *et al.*, 2016). The

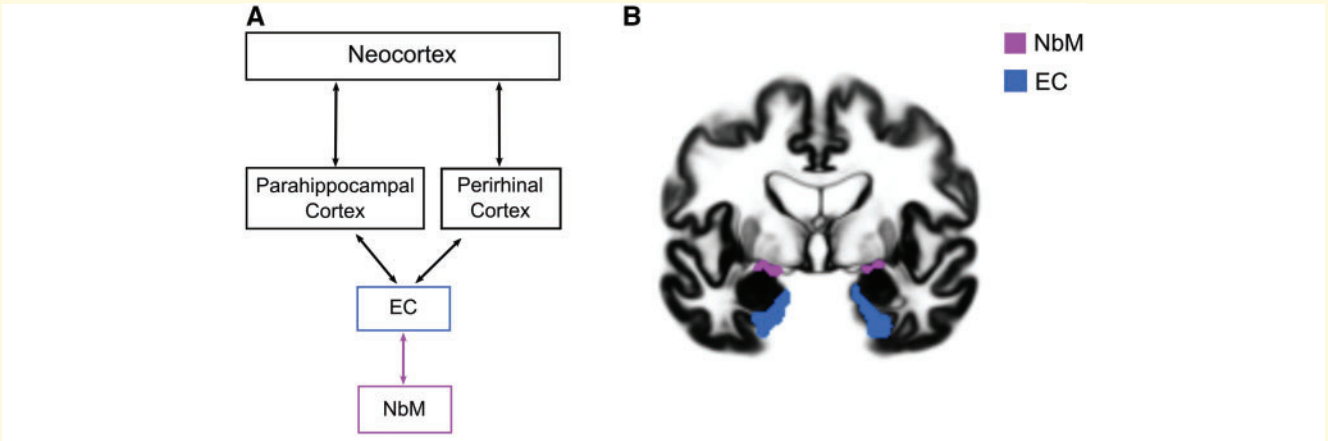

Figure 1 Proposed basal forebrain→entorhinal→neocortical model and regions of interest. (**A**) Predictive pathological staging model of tau pathology originating in entorhinal cortex (EC) and spreading via trans-synaptic mechanism to cortical targets of its projection system (black squares) updated to incorporate the basal forebrain degeneration as an 'upstream' event in the pathological cascade (purple square). (**B**) Regions of interest of the NbM (purple) and the entorhinal cortex (blue) are superimposed on a coronal slice of the population DARTEL template. (**A**) is adapted with permission from Liu *et al.* (2012).

patterns of tau propagation in mice parallel patterns of grey matter loss observed in human *in vivo* imaging studies, proving an underlying molecular-level mechanism that might drive neurodegenerative spreading dynamics in the entorhinal cortex (EC)→Neocortical model (Fig. 1A).

Challenging the EC→Neocortical model, we have previously demonstrated that the magnitude of early longitudinal grey matter loss in the NbM was larger than in the entorhinal cortex in cognitively normal older adult humans exhibiting abnormal CSF biomarkers of amyloid-β accumulation (Schmitz and Spreng, 2016). We also found that baseline NbM volumes were predictive of future rates of longitudinal structural degeneration in entorhinal cortex, raising the possibility that amyloid-β accumulation potentiates the spread of pTau via the same trans-synaptic mechanisms proposed previously in mouse models of Alzheimer's disease (de Calignon *et al.*, 2012; Liu *et al.*, 2012; Khan *et al.*, 2014; Wu *et al.*, 2016). If true, the NbM→EC model would add a crucial 'upstream' link to the EC→Neocortical predictive pathological staging of Alzheimer's disease. Under this model, amyloid-β pathology in the ascending cholinergic projections from NbM first 'seed' the entorhinal cortex with pTau via trans-synaptic spread, thereby eventuating the pattern of temporo-parietal neurodegeneration typically attributed to the earliest stages of Alzheimer's disease. Support for the NbM→EC model would have major clinical implications, motivating a shift towards preventative treatment strategies aimed at relieving age-related pressures on the cortical cholinergic projection system.

However, our prior evidence in support of the NbM→EC neurodegenerative 'spread' model is provisional. Like most predictive staging studies in humans, we only examined a single large heterogeneous cohort of older adults. A stronger test of this model requires a systematic replication using identical multimodal analytical procedures, between two large independent cohorts. Moreover, the molecular profile of background proteinopathy will need to incorporate both amyloid-β and pTau, as opposed to amyloid-β alone (Schmitz and Spreng, 2016), in order to better match the pathophysiological conditions that are hypothesized to drive the initial trans-synaptic spreading of pTau across interconnected brain regions. Finally, a test of the EC→Neocortical model is needed within this same study to determine if neocortical 'targets' predicted by entorhinal cortex neurodegeneration are similar to neocortical targets predicted by entorhinal cortex trans-synaptic spreading (de Calignon *et al.*, 2012; Liu *et al.*, 2012; Khan *et al.*, 2014; Wu *et al.*, 2016). This would provide an important validation that our non-invasive *in vivo* analyses index a common pathophysiological mechanism to those observed in rodent models.

Here we directly compared the NbM→EC and EC→NbM models of predictive pathological staging in a large sample of older adults ranging from cognitively normal to Alzheimer's dementia, and then examined if the results generalized to a second independent sample of adults spanning the same clinical diagnostic continuum. In each sample, we first integrated CSF biomarkers of amyloid-β and pTau neuropathology into a ratio of pTau/amyloid-β and delineated two groups of older adults in each of the two samples using an independently defined cut-off point that was recently cross-validated for the ratio of pTau/amyloid-β (Hansson *et al.*, 2018; Schindler *et al.*, 2018). Individuals below the cut-off point exhibit a 'neurotypical' pTau/amyloid-β phenotype of brain ageing; individuals above the cut-off point exhibit an 'Alzheimer's pathological' pTau/amyloid-β phenotype. Because CSF pTau/amyloid-β is sensitive to the earliest abnormalities of Alzheimer's disease (Jack *et al.*, 2013), we identified many cognitively normal adults falling above the cut-off

point in both samples. The Alzheimer's pathological pTau/amyloid-β phenotype therefore captures 'pre-symptomatic' individuals, in addition to mild cognitive impairment (MCI) and Alzheimer's disease individuals. In each sample, we then tracked the two CSF groups with structural MRI indices of baseline grey matter volume and longitudinal neurodegeneration over a 2-year period. Both the CSF and structural MRI data were acquired from multiple phases of the Alzheimer's Disease Neuroimaging Initiative (ADNI).

To examine the 'spread' of degeneration between NbM and entorhinal cortex, we used a predictive modelling strategy which tests whether baseline grey matter volume in a seed region accounts for variation in subsequent longitudinal degeneration (change over future time points) in a target region. We determined whether evidence of predictive pathological spread favoured either the NbM→EC or EC→NbM model. We then determined whether CSF concentrations of pTau/amyloid-β moderated the observed predictive relationship, consistent with an underlying trans-synaptic mechanism of pathophysiological spread. Additional moderating factors, including clinical diagnosis, were evaluated in this framework. We then examined the selectivity of predictive pathological spread between NbM and entorhinal cortex using a whole-brain voxel-wise predictive modelling strategy. Finally, we used the same whole-brain strategy to test whether the EC→Neocortical model recapitulates the spread of neuropathology from entorhinal cortex to temporoparietal cortices observed in prior cross-species translational work (de Calignon *et al.*, 2012; Liu *et al.*, 2012; Khan *et al.*, 2014; Wu *et al.*, 2016). If degeneration in the basal forebrain cholinergic projection system is a robust and reliable upstream event of entorhinal degeneration, then it should predict localized entorhinal degeneration, whereas entorhinal cortex should predict downstream events in temporal and parietal cortices.

Materials and methods

ADNI data

Data used in the preparation of this article were obtained from the Alzheimer's Disease Neuroimaging Initiative (ADNI) database (adni.loni.usc.edu). The ADNI was launched in 2003 as a public-private partnership, led by principal investigator Michael W. Weiner, MD (Mueller *et al.*, 2005). The primary goal of ADNI has been to test whether serial MRI, PET, other biological markers, and clinical and neuropsychological assessment can be combined to measure the progression of MCI and early Alzheimer's disease.

We used data from the ADNI-1 as the first cohort and the combined data from ADNI-GO and ADNI-2 (ADNI-GO/2) as the second cohort. ADNI-1 was carried out in 1.5 T magnetic resonance scanners and ADNI-GO/2 in 3 T magnetic resonance scanners. All high-resolution T_1 structural MRI scans were downloaded from ADNI LONI (http://adni.loni.usc.edu/). A total of 502 ADNI-1 structural MRI scans were downloaded from a standardized 2-year interval image collection. This data collection was created to minimize variability between studies and ensure a minimum quality control of the images (Wyman *et al.*, 2013). To obtain the ADNI-GO/2 structural MRI scans, we first selected those subjects who had CSF biomarker data (see below) and searched by their research IDs (RIDs). We downloaded longitudinal structural MRI images from 714 ADNI-GO/2 participants. To select the two longitudinal time points for each individual, we applied a bounded interval of a mean = 1.5 years ± 12 months to maximize the inclusion of participants. One hundred and four participants did not have longitudinal structural MRI data within the bounded interval. For ADNI sites with GE and Siemens scanners, we used images corrected for distortions (GradWarp) and B1 non-uniformity. For ADNI sites with Philips scanners, these corrections are applied at acquisition (see http://adni.loni.usc.edu/methods/mri-tool/mri-pre-processing/). Finally, to be able to compare ADNI-1 and ADNI-GO/2 data as two independent samples, we discarded participants from ADNI-GO/2 who also took part in the ADNI-1 studies ($n = 49$), due to the smaller sample size of the ADNI-1 cohort.

CSF biomarkers

Accumulation of brain amyloid-β in plaques and pTau in neurofibrillary tangles are the main proteinopathies associated with Alzheimer's disease (Shaw *et al.*, 2009; Hansson *et al.*, 2018; Schindler *et al.*, 2018). CSF samples of amyloid-β and pTau from the baseline visit were produced with a fully automated Elecsys® protocol (Supplementary material). We calculated a ratio of pTau/amyloid-β and used a standardized cut-off of 0.028, which was recently cross-validated between the ADNI and Swedish BioFinder studies (Hansson *et al.*, 2018) to classify participants into abnormal (pTau/amyloid-β $\geqslant$ 0.028) and normal (pTau/amyloid-β $<$ 0.028) CSF groups. Using ratios of pTau/amyloid-β supersedes using single analytes to distinguish amyloid status using PET (Schindler *et al.*, 2018). Moreover, in the ADNI dataset, a high concordance was found between this CSF pTau/amyloid-β cut-off point and amyloid PET cut-off points (Hansson *et al.*, 2018). Two hundred and sixteen participants from ADNI-1 did not have CSF measures and were therefore not included. It is important to note that our grouping strategy is purely based on CSF biomarkers, independent of any cognitive or clinical diagnosis, though we follow-up with analyses of clinical diagnosis (refer to the 'Results' section).

APOE genotyping

The ε4 allele of the *APOE* gene is the strongest genetic risk factor for non-familial Alzheimer's disease (Corder *et al.*, 1993; Strittmatter *et al.*, 1993; Farrer *et al.*, 1997) and is thought to interact with the selective vulnerability of cholinergic basal forebrain neurons by disrupting the capacity of these cells to support and maintain their enormous axonal membranes (Wurtman *et al.*, 1990; Nitsch *et al.*, 1992; Wurtman, 1992; Poirier *et al.*, 1993, 1995; Poirier, 1994). To study the effect of the CSF Alzheimer's disease biomarkers independently of other factors, we included the *APOE* genotype as a covariate of no interest in our analyses. The *APOE* information for all individuals with both structural MRI and CSF data was obtained from the APOERES.csv spreadsheet and the ε4+ status was defined as having at least one ε4 allele. A blood

sample at the screening or baseline visit was collected for *APOE* genotyping and genotype analysis was performed following standard procedures (Saykin *et al.*, 2010).

Neuropsychological assessment

Cognitive performance was assessed with a neuropsychological battery that covered a wide range of cognitive functions, including short and long-term memory, language, executive function and attention. We used baseline data from two composite scores, one for memory and one for executive function, derived from the ADNI neuropsychological battery that were recently validated using confirmatory factor analysis (Crane *et al.*, 2012; Gibbons *et al.*, 2012). Specifically, the memory score integrated the Mini-Mental State Examination (MMSE), Rey Auditory Verbal Learning Test, Alzheimer's Disease Assessment Scale, and Logical Memory tests. The executive function score integrated the Category Fluency, Digit Span Backwards, Digit Symbol Substitution, Trails A and B and Clock Drawing tests. In addition to the memory and executive function factors, we present the Boston Naming and the Clock Drawing tests and the six subcategories of the Clinical Dementia Rating (CDR) Scale to provide a more comprehensive evaluation of the cognitive and functional profiles of the participants. The CDR subtests include the domains of Memory, Orientation, Judgement and Problem Solving, Community Affairs, Home and Hobbies and Personal Care.

ADNI clinical diagnosis

At the baseline visit, an initial diagnosis recommended by the ADNI Clinical Core was used to classify participants into cognitively normal (CDR = 0, MMSE 24–30), mild cognitively impaired (CDR = 0.5, MMSE 24–30, with memory impairments but largely preserved general cognition and functional capacity) and Alzheimer's disease (CDR 0.5–1, MMSE 20–26, with memory impairments but largely impaired general cognition and functional capacity). These diagnostic classifications are based on standard cognitive and functional measures typical of clinical trials (Aisen *et al.*, 2010, 2015; Petersen *et al.*, 2010). More details on the inclusion and diagnostic criteria can be found at http://adni.loni.usc.edu/.

CSF groups by neuropsychological status

To confirm that our CSF grouping strategy differentiated participants based on measures of neuropsychological status, we collapsed the baseline neuropsychological data from both ADNI cohorts to compare the abnormal and normal CSF groups on the MMSE, a common test of general cognitive function, in the two composite scores of memory and executive function as well as in the Boston Naming Test, Clock Drawing Test and in the CDR subcategories (see preceding section). For each test, we computed one-way fixed effect ANOVAs with CSF group (abnormal CSF, normal CSF) as a factor, covarying for age, sex, education, cohort and *APOE* genotype. These models revealed significant main effects of CSF pathology on cognition in all tests. Consistent with the sensitivity of CSF pTau/amyloid-β to pathological ageing, the abnormal CSF group exhibited significantly more cognitive impairment than the normal CSF group in all the tests (Table 1).

Longitudinal structural MRI

A serial longitudinal pipeline scheme in SPM12 r7219 (https://www.fil.ion.ucl.ac.uk/spm/) implemented in MATLAB 2013a was used to calculate the grey matter volume changes from the structural MRI data (Ashburner and Ridgway, 2012). This procedure unifies rigid-body registration, intensity inhomogeneity correction and non-linear diffeomorphic transformation in a single iterative model. Initially, all of the individual time points were co-registered to the ICBM 152 volume to ensure good starting parameters for the high-dimensional DARTEL warping algorithm. We then used within-subject symmetric diffeomorphic registration of the two time points to create a midpoint average T_1 image for each subject. Computing a midpoint average image prevents introduction of biases associated with using individual time points as the reference (e.g. results differ depending on the time point that is used as a reference). The midpoint average was scaled by the interscan interval. The registration step produced Jacobian determinant maps, which index contractions and expansions for each time point relative to the midpoint average image. The default parameters for noise estimation, warping and bias regularizations were used. The midpoint average images were then segmented using the SPM12 tissue probability map with the following settings: light regularization, 60 mm of full-width at half-maximum (FWHM) Gaussian smoothness of bias and 2, 2, 2, 3, 4, 2 Gaussians per tissue type. The resulting 1.5 mm^3 grey and white matter maps were used to create separate DARTEL group templates for each sample (ADNI-1 and ADNI-GO/2). The DARTEL algorithm improves the intersubject alignment by using multiple parameters per voxel when aligning the images (Ashburner, 2007). The segmented grey matter maps were multiplied by the Jacobian determinants of each time point (Mechelli *et al.*, 2005). We then warped the segmented grey and white matter maps into the DARTEL template space with the 'preserve amount' option. Default settings were used elsewhere. The warping step produced modulated grey and white matter volumetric maps for each time point.

To check the quality of the images for subsequent analyses, the warped, modulated grey matter maps of each time point were visually inspected for segmentation and normalization inaccuracies by creating a plot showing a slice for all the subjects and were inspected for the presence of outliers by calculating the correlation between all the volumes using the CAT12 toolbox (http://dbm.neuro.uni-jena.de/cat/). Subjects who exhibited a correlation below 2 standard deviations (SD) and abnormalities on their segmented grey matter volume (e.g. low signal intensity, inhomogeneities, warping errors) were excluded. Two subjects were discarded because of low data quality in ADNI-1 and eight in ADNI-GO/2. See Table 2 for complete information of the included participants.

Region of interest definition

To test the predictive pathological models between the NbM and entorhinal cortex, we extracted grey matter volumes from two regions of interest using probabilistic atlases. The NbM and entorhinal cortex regions of interest were bilateral (combined across hemispheres) and were created in MNI space with

Table 1 Neuropsychological function at baseline by CSF group (collapsed across ADNI cohorts)

	CSF group		*F*	*P*
	Abnormal CSF	Normal CSF		
MMSE	26.28 (2.83)	28.65 (1.57)	$F(1,830) = 112.74$	<0.001*
Memory function	–0.19 (0.81)	0.86 (0.68)	$F(1,829) = 243.77$	<0.001*
Executive function	–0.20 (1.01)	0.72 (0.88)	$F(1,829) = 123.96$	<0.001*
BNT	25.28 (4.71)	27.48 (3.19)	$F(1,818) = 30.28$	<0.001*
Clock-Draw	3.98 (1.18)	4.57 (0.72)	$F(1,829) = 37.26$	<0.001*
CDR-MEM	0.64 (0.43)	0.19 (0.28)	$F(1,830) = 173.80$	<0.001*
CDR-ORIENT	0.43 (0.46)	0.06 (0.18)	$F(1,830) = 113.30$	<0.001*
CDR-JUDGE	0.45 (0.39)	0.11 (0.22)	$F(1,830) = 136.57$	<0.001*
CDR-COMMUN	0.32 (0.41)	0.05 (0.16)	$F(1,830) = 86.47$	<0.001*
CDR-HOME	0.37 (0.46)	0.07 (0.20)	$F(1,830) = 83.26$	<0.001*
CDR-CARE	0.09 (0.29)	0.01 (0.11)	$F(1,830) = 9.98$	0.001*

Mean (SD) of the neuropsychological baseline performances. The abnormal CSF group exhibited worse general cognition (MMSE), memory, executive function, naming, visuospatial functions and in all subtests of the Clinical Dementia Rating (CDR) scale compared to the normal CSF group. Total scores are reported for the Boston Naming and Clock Drawing Tests. BNT = Boston Naming Test; CDR-CARE = CDR personal care domain; CDR-COMMUN = CDR community affairs domain; CDR-HOME = CDR home and hobbies domain; CDR-JUDGE = CDR judgement and problem solving domain; CDR-MEM = CDR memory domain; CDR-ORIENT = CDR orientation domain; MMSE = Mini-Mental State Examination.

*Significant after Bonferroni correction at $P < 0.05$ ($n = 11$ tests).

Table 2 Participant demographics, *APOE* genotype and CSF assays

	ADNI-1			ADNI-GO/2		
	Abnormal CSF	Normal CSF	Test	Abnormal CSF	Normal CSF	Test
n (total)	174	110	$\chi^2 = 14.42^{***}$	316	237	$\chi^2 = 11.28^{***}$
CN/MCI/AD	28/89/57	64/41/5	$\chi^2 = 64.26^{***}$	39/130/147	162/75/0	$\chi^2 = 230.84^{***}$
Age	74.51 (7.04)	75.53 (6.50)	$t = -1.24$	72.16 (7.22)	70.44 (6.56)	$t = 2.91^{**}$
Female/male	66/108	50/60	$\chi^2 = 1.28$	146/170	110/127	$\chi^2 = 0.00$
Education	15.57 (2.99)	15.88 (2.89)	$t = -0.87$	15.96 (2.66)	16.62 (2.56)	$t = 2.96^{**}$
ε4+/ε4–	124/50	16/94	$\chi^2 = 84.48^{***}$	222/94	60/177	$\chi^2 = 107.54^{***}$
Amyloid-β	579.28 (179.15)	1468.76 (554.28)	$t = -16.30^{***}$	641.66 (192.73)	1376.54 (589.78)	$t = -18.45^{***}$
pTau	34.33 (12.33)	19.6 (6.45)	$t = 13.16^{***}$	35.75 (14.98)	18.23 (6.52)	$t = 18.57^{***}$

Information of the included participants from the ADNI-1 and ADNI-GO/2 cohorts by CSF group. Values represent mean (SD) unless otherwise specified. Aβ = CSF concentration of the amyloid beta 1-42 peptide; pTau = CSF concentration of hyper phosphorylated tau (at threonine 181). Independent samples *t*-tests (*t*) and chi-square (χ^2) tests were used to test CSF group differences within each ADNI cohort. Baseline clinical diagnosis: AD = Alzheimer's disease; CN = cognitively normal; MCI = mild cognitively impaired. *APOE* status: ε4+ = ε4 carrier, ε4– = ε4 non-carrier. Age and education are in years. Amyloid-$\beta_{1\text{-}42}$ and pTau concentrations are in pg/ml. $^{***}P < 0.001$, $^{**}P < 0.005$.

the SPM Anatomy Toolbox r 2.2b (http://www.fz-juelich.de/inm/inm-1/DE/Forschung/) using previously published probabilistic maps of the NbM (Zaborszky *et al.*, 2008) and the entorhinal cortex (Amunts *et al.*, 2005) (Fig. 1B). The NbM region of interest is equivalent to areas Ch4 and Ch4p (Mesulam *et al.*, 1983*a*, *b*; Mesulam and Geula, 1988). The Ch4p area is also referred to as the nucleus subputaminalis of Ayala and represents the rostrolateral extension of the NbM. Research by others on the subregional degeneration within the distributed nuclei of the basal forebrain has highlighted the Ch4p region as particularly vulnerable to early degeneration in amnestic MCI (Teipel *et al.*, 2005, 2014; Grothe *et al.*, 2012; Kilimann *et al.*, 2014). Because of their neuroanatomical proximity to one another and higher susceptibility to Alzheimer's disease neurodegeneration, we have considered the Ch4p and Ch4 regions as a single unit. The regions of interest were thresholded at 50% probability (minimum overlap of 5/10 post-mortem brains). The regions of interest were then resampled and warped to the DARTEL group template (Fig. 1B). Estimates of modulated grey matter volume (in units of ml) at each time point were obtained using the region of interest as a masking region, and by summing the total intensity of voxels falling within the masking region adjusted for the size and number of voxels (http://www0.cs.ucl.ac.uk/staff/g.ridgway/vbm/get_totals.m). No spatial smoothing was applied to the volumes. In addition, the total grey matter from the modulated and warped individual time points was calculated using the same procedure. The total intracranial volume (TICV) was computed by summing up the tissue volumes of grey matter, white matter and CSF of the segmented average images produced in a previous step using the *seg8.mat file from the segmentation (Malone *et al.*, 2015).

To assess longitudinal changes in grey matter volumes, the annualized per cent change (APC) from baseline was calculated using Equation 1 (Cavedo *et al.*, 2017):

$$APC = \left(\frac{change\ baseline\ (ml)}{value\ baseline\ (ml)}\right) \times \left(\frac{365}{interscan\ interval\ (days)}\right) \times 100 \quad (1)$$

Statistical analyses

ANOVA

To compare baseline volumes and longitudinal volume changes between the CSF groups, we computed fixed effects ANOVAs for each ADNI cohort and each region of interest with CSF group (abnormal CSF, normal CSF) as a factor covarying for age, sex, education, TICV, baseline total grey matter and *APOE* genotype (see Supplementary Fig. 1 for the bivariate correlation values among the modelled variables). We then pooled the data from both ADNI cohorts and computed one-way fixed effects ANOVAs with CSF group (abnormal CSF, normal CSF) as a factor, correcting for the same covariates, and an additional covariate for study cohort (Ma *et al.*, 2019). All ANOVA models were carried out in R with a type III sums of squares.

Robust regression

To test the predictive staging models (NbM→EC and EC→NbM), robust linear regression analyses were carried out in Matlab R2018b with *filtm* and a bisquare weight function to minimize the influence of outliers. Each model covaried for age, sex, education, TICV, baseline total grey matter and *APOE* genotype. The predictive models were calculated first for each dataset separately and then in the pooled sample collapsing across both cohorts and including an additional covariate for cohort. All data were *z*-scored before entering the analysis.

Moderation analyses of independent samples

The moderation analyses (Fig. 3E and J) were carried out using the PROCESS macro for SPSS (Hayes, 2017). The abnormal and normal CSF groups served as the dichotomous moderator variable in all models. Age, sex, education, TICV, baseline total grey matter, *APOE* genotype and cohort were included as covariates in all models. All data were mean centred. The moderation analysis used a heteroscedasticity consistent standard error and covariance matrix estimator.

Comparison of correlations between dependent samples

To compare correlation coefficients between the NbM→EC and EC→NbM models, we used *cocor* to account for the dependence between the two models (Diedenhofen and Musch, 2015).

Whole-brain analysis

Whole-brain APC maps were calculated with the previous APC formula with the *imcalc* tool in SPM12. The APC maps were smoothed with a 4 mm FWHM Gaussian kernel (Grothe *et al.*, 2012; Cavedo *et al.*, 2017). For exploratory purposes, we tested two whole-brain models. The first model investigated the anatomical specificity of the relationship between baseline NbM volumes and longitudinal degeneration in the entorhinal cortex using whole-brain voxel-wise analysis. The second model investigated the relationship between baseline EC volumes and longitudinal degeneration in adjacent medial temporal cortices using whole-brain voxel-wise analysis. Both models were evaluated in the abnormal CSF group pooled across the ADNI-1 and ADNI-GO/ADNI-2 datasets. These regression models were estimated with non-parametric permutation testing using the Statistical Non-Parametric Mapping toolbox v13 (http://warwick.ac.uk/snpm) for SPM12 (Nichols and Holmes, 2002). Age, sex, education, TICV, baseline total grey matter, *APOE* genotype and cohort were included as covariates. The models were estimated with 5000 permutations, without variance smoothing and global normalization, and including an explicit mask of the binarized and thresholded (>0.1) DARTEL grey matter ADNI-GO/2 group template. Results are presented with a voxel-level threshold of $P < 0.05$ family-wise error (FWE) corrected for multiple comparisons across the brain.

Data availability

The data that support the findings of this study are openly available for request in LONI https://ida.loni.usc.edu/login.jsp.

Results

Abnormal CSF pTau/amyloid-β differentiates MRI indices of NbM and entorhinal cortex neurodegeneration

We first examined whether the CSF pTau/amyloid-β grouping criteria differentiates patterns of baseline NbM and entorhinal cortex volume. Consistent with a link between CSF pTau/amyloid-β biomarkers of neuropathology and neurodegeneration, we found that individuals with abnormal CSF cut-offs had smaller baseline volumes in the NbM in the ADNI-1 [main effect of CSF Group: $F(1,276) = 9.04$, $P = 0.002$, $\eta^2 = 0.013$], ADNI-GO/2 [main effect of CSF Group: $F(1,545) = 67.01$, $P < 0.001$, $\eta^2 = 0.042$] and in the pooled data of both cohorts [main effect of CSF Group: $F(1,828) = 75.88$, $P < 0.001$, $\eta^2 = 0.030$; Fig. 2A]. Baseline volumes of the entorhinal cortex were also smaller in the abnormal CSF group in ADNI-1 [main effect of CSF Group: $F(1,276) = 8.71$, $P = 0.003$, $\eta^2 = 0.012$], ADNI-GO/2 [main effect of CSF Group: $F(1,545) = 14.19$, $P < 0.001$, $\eta^2 = 0.008$] and in the pooled data [main effect of CSF Group: $F(1,828) = 25.86$, $P < 0.001$, $\eta^2 = 0.010$; Fig. 2C].

We next examined if the CSF pTau/amyloid-β grouping criteria also influenced longitudinal indices of APC in the NbM and entorhinal cortex. These models revealed that individuals with abnormal CSF biomarkers showed more longitudinal atrophy in the NbM in the ADNI-GO/2 [main effect of CSF Group: $F(1,545) = 7.89$, $P = 0.005$, $\eta^2 = 0.014$] and in the pooled dataset [main effect of CSF Group: $F(1,828) = 9.79$, $P = 0.002$,

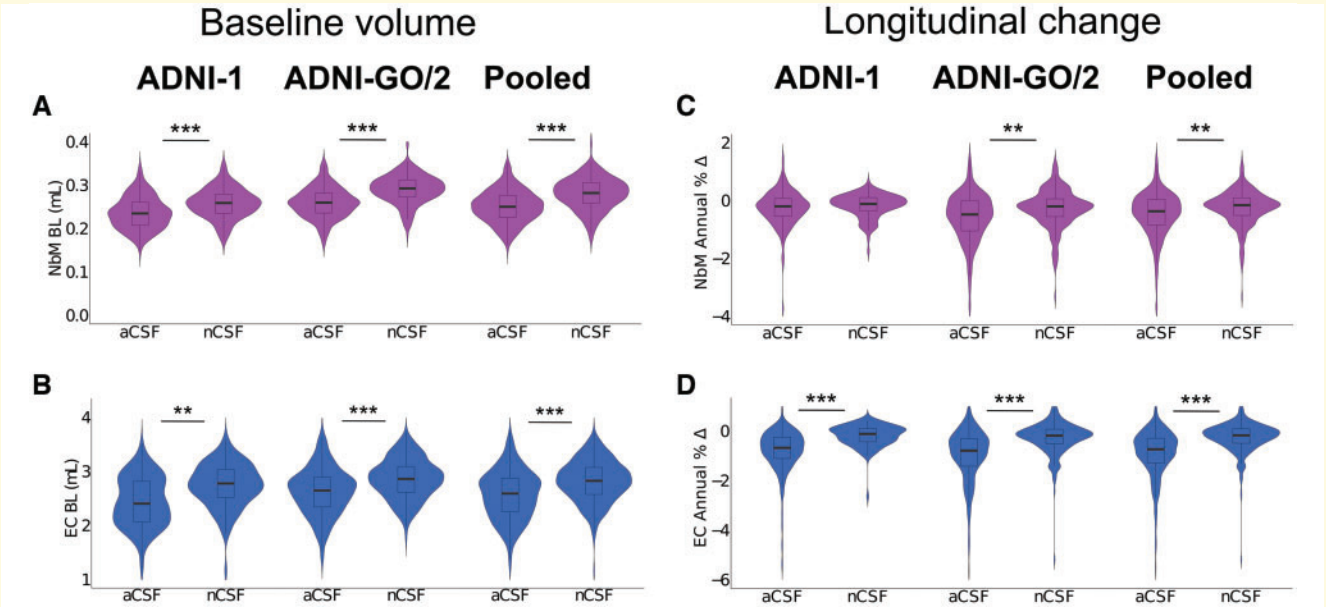

Figure 2 Abnormal pTau/amyloid-β differentiates NbM and entorhinal cortex indices of structural degeneration. Violin plots showing the means and standard errors of the baseline and longitudinal changes of the NbM (purple bars) and entorhinal cortex (EC, blue bars) *a priori* regions of interest in the two independent datasets (ADNI-1 and ADNI-GO/2) and the pooled data of both datasets. Baseline NbM (**A**) and entorhinal cortex (**C**) volumes were smaller in the abnormal CSF (aCSF) group. Longitudinal degeneration in the NbM (**B**) and in the entorhinal cortex (**D**) was larger in the abnormal CSF group. BL = baseline volume. $^{***}P < 0.001$; $^{**}P < 0.01$; $^{*}P < 0.05$. Horizontal lines are the median, boxes are interquartile range and vertical lines are 1.5× the interquartile range.

$\eta^2 = 0.011$], but not in ADNI-1 [main effect of CSF Group: $F(1,276) = 2.54$, $P = 0.11$, $\eta^2 = 0.009$; Fig. 2B]. In the entorhinal cortex, the abnormal CSF group exhibited more longitudinal atrophy in ADNI-1 [main effect of CSF Group: $F(1,276) = 23.91$, $P < 0.001$, $\eta^2 = 0.072$], ADNI-GO/2 [main effect of CSF Group: $F(1,545) = 26.38$, $P < 0.001$, $\eta^2 = 0.041$] and in the pooled data [main effect of CSF Group: $F(1,828) = 47.51$, $P < 0.001$, $\eta^2 = 0.048$; Fig. 2D]. Finally, we investigated if the magnitude of longitudinal degeneration in the NbM and in the entorhinal cortex differed between individuals at different disease stages. To do so, we cross-referenced the CSF groups with the ADNI baseline clinical diagnosis (Schmitz and Spreng, 2016; Schmitz *et al.*, 2018) and found that individuals with abnormal CSF biomarkers in all disease stages had increased degeneration in both the NbM and the entorhinal cortex. Crucially, individuals in the preclinical disease stage (abnormal CSF and normal cognition at baseline) showed greater magnitudes of degeneration in the NbM and the entorhinal cortex compared to the cognitively normal controls (normal CSF and normal cognition at baseline) (Supplementary Fig. 2 and Supplementary Table 1). Consistent with our hypotheses, CSF biomarkers of abnormal pTau/amyloid-β accumulation in the CNS differentiated both smaller baseline grey matter volume and larger magnitudes of longitudinal grey matter degeneration in the NbM and entorhinal cortex.

Abnormal pTau/amyloid-β potentiates the predictive spread of NbM→EC degeneration

Thus far, our multimodal CSF and structural MRI analyses have treated patterns of neurodegeneration in the NbM and entorhinal cortex separately. We next used regression-based modelling to test if the degeneration in the NbM and in the entorhinal cortex reflects interdependent pathological processes. If degeneration in the NbM precedes degeneration in the entorhinal cortex due to selective neuronal vulnerability of cholinergic neurons inducing a degenerative 'spreading,' then NbM baseline volumes should predict degeneration in the entorhinal cortex (NbM→EC). However, if degeneration in NbM and entorhinal cortex occurs in parallel due to a common global pathology, then baseline volumes of either region should predict degeneration in the other. Alternatively, if degeneration in NbM and entorhinal cortex reflects independent local pathology, then baseline volumes of neither region should predict degeneration in the other.

We used robust linear regression to examine these competing models in the abnormal and normal CSF groups. Consistent with an interdependent NbM→EC model, we found in the abnormal CSF group that baseline NbM volumes predicted longitudinal degeneration in the entorhinal cortex in both ADNI-1 [r = 0.20, $t(166) = 2.12$, $P = 0.03$, confidence interval (CI): 0.01 to 0.38; Fig. 3A] and ADNI-

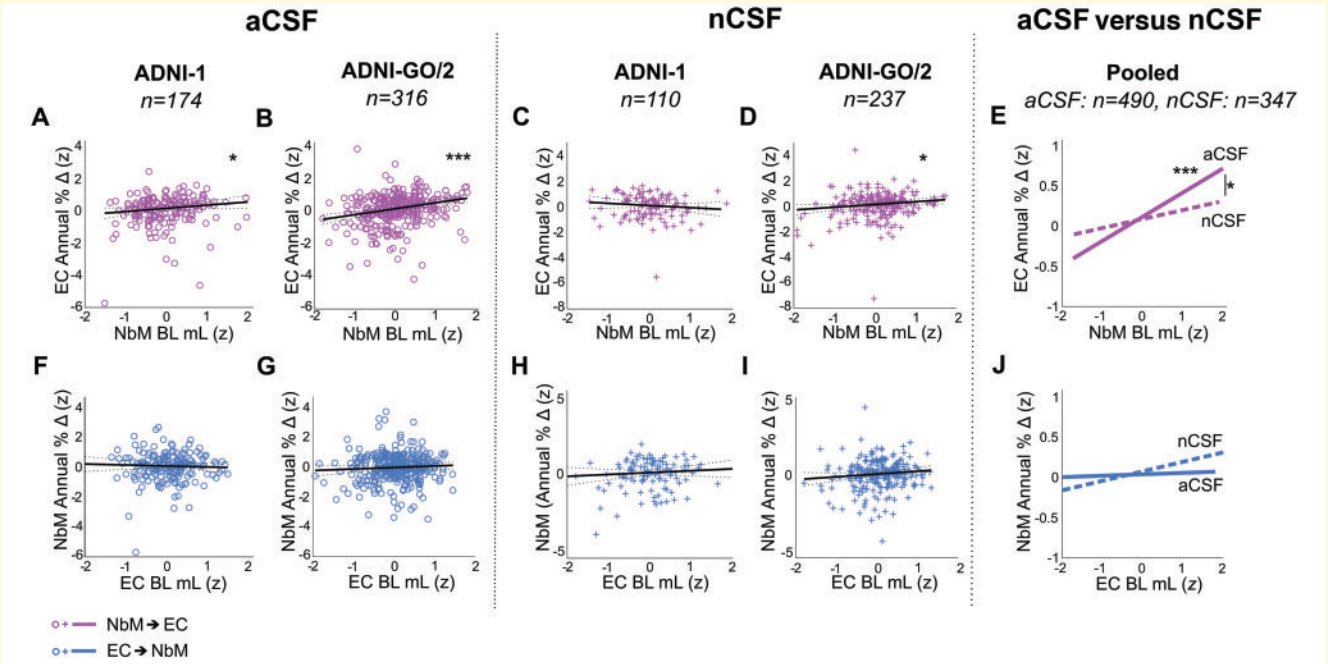

Figure 3 Predictive pathological staging models. In the abnormal CSF group (aCSF), smaller baseline NbM volumes (*x*-axis: negative z-score values) were associated with greater magnitudes of longitudinal degeneration in the entorhinal cortex (*y*-axis: negative z-score values for T_2 – T_1 APC) in both (**A**) ADNI-1 and (**B**) ADNI-GO/2 (*lower left* corner of the graphs). No such relationships were observed in the normal CSF (nCSF) groups in (**C**) ADNI-1 but it was present in (**D**) ADNI-GO/2. (**E**) CSF concentrations of pTau/amyloid-β (normal CSF versus abnormal CSF) significantly moderated the relationship between baseline NbM volume and longitudinal entorhinal cortex degeneration. (**F**–**J**) Baseline entorhinal cortex volumes did not predict longitudinal degeneration in the NbM in either the abnormal or normal CSF, in either ADNI-1 or ADNI-GO/2. nor did it moderate this relationship. BL = baseline volume. $^{***}P < 0.001$; $^{**}P < 0.01$; $^{*}P < 0.05$.

GO/2 [r = 0.37, $t(308) = 5.15$, $P < 0.001$, CI: 0.22 to 0.51; Fig. 3B]. We next examined whether the predictive pathological staging of NbM and entorhinal cortex degeneration is observable under conditions of normal CSF pTau/amyloid-β. It could be the case that the underlying neuropathological process driving this relationship also occurs at 'neurotypical' levels of pTau/amyloid-β, but that this process is exacerbated in the abnormal CSF group. In this case, we would expect to observe the same NbM→EC interrelationship, though possibly at a smaller magnitude. We found negligible evidence for the NbM→EC model in the normal CSF group in ADNI-1 [r = –0.17, $t(102) = -1.14$, $P = 0.25$, CI: –0.46 to 0.12; Fig. 3C]. However, we did observe a predictive relationship in ADNI-GO/2 [r = 0.21, $t(229) = 2.47$, $P = 0.01$, CI: 0.04 to 0.39; Fig. 3D]. We then examined these relationships in the pooled data. The results supported the NbM→EC model in the abnormal CSF [r = 0.30, $t(481) = 5.32$, $P < 0.001$, CI: 0.19 to 0.41] but not the normal CSF group [r = 0.11, $t(338) = 1.45$, $P = 0.14$, CI: –0.04 to 0.26] (Fig. 3E and Supplementary Table 2). To exclude the possibility that the results were distorted by possible collinearities among the model predictors and covariates, we computed each model without any of the covariates. The exclusion of covariates did not alter any of the above findings (Supplementary Table 3). To directly test if the relationship observed in the pooled abnormal CSF group was significantly different from that observed in the pooled normal CSF group, we computed a moderation analysis with CSF group (abnormal, normal) as a dichotomous moderator on the NbM→EC interrelationship (refer to the 'Materials and methods' section). We found a significant moderating effect of CSF group on the NbM→EC interrelationship [$t(826) = 2.55$, $P = 0.01$], indicating a more pronounced interregional spread in the abnormal CSF compared to the normal CSF group.

We next tested the competing model of EC→NbM predictive pathological spread, focusing first on the abnormal CSF group. We found that entorhinal cortex baseline volumes did not predict longitudinal decreases in the NbM in ADNI-1 [r = –0.06, $t(166) = -0.56$, $P = 0.57$, CI: –0.29 to 0.16; Fig. 3F], in ADNI-GO/2 [r = 0.10, $t(308) = 1.18$, $P = 0.23$, CI: –0.06 to 0.27; Fig. 3G] or in the pooled sample [r = 0.02, $t(481) = 0.26$, $P = 0.79$, CI: –0.11 to 0.14; Fig. 3J] (Supplementary Table 2). Moreover, we found negligible evidence for the EC→NbM model in the normal CSF group in ADNI-1 [r = 0.12, $t(102) = 0.92$, $P = 0.36$, CI: –0.14 to 0.38; Fig. 3H], ADNI-GO/2 [r = 0.18, $t(229) = 1.72$, $P = 0.08$, CI: –0.03 to 0.40; Fig. 3I], or in the pooled sample [r = 0.12, $t(334) = 1.53$,

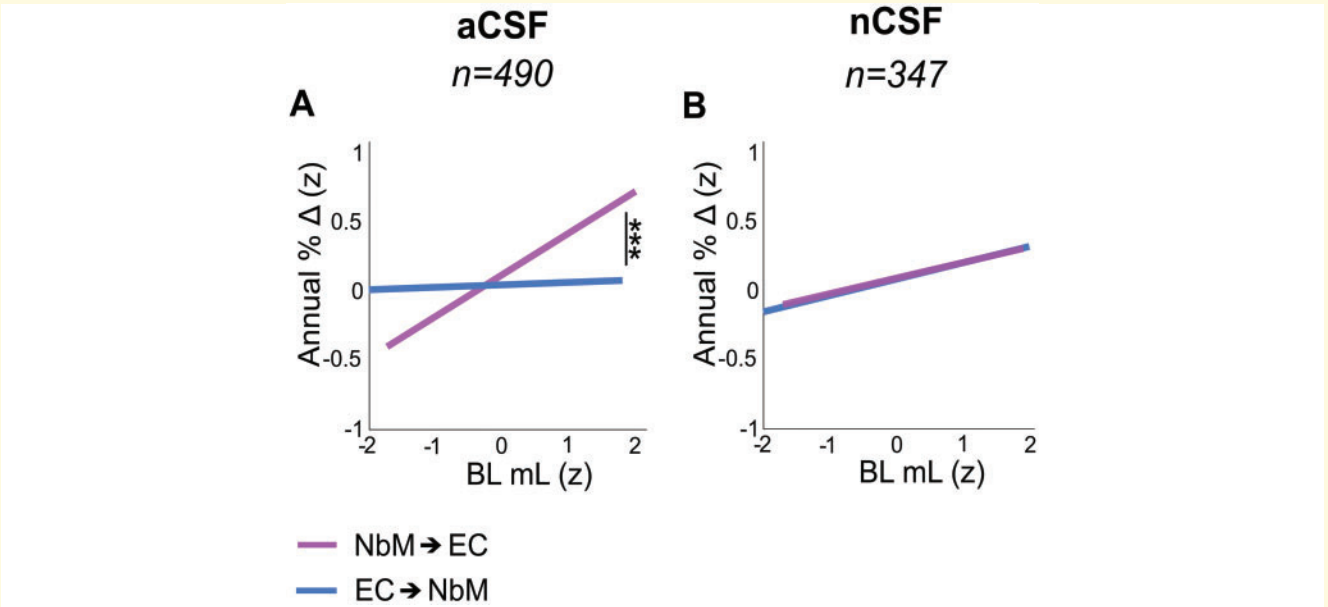

Figure 4 Amyloid-β and pTau potentiate the spread of neurodegeneration from NbM to entorhinal cortex. The slopes of the NbM→EC and EC→NbM robust regression models were different in (**A**) the pooled abnormal CSF group (aCSF), but (**B**) not in the pooled normal CSF group. The *x*-axes reflect baseline NbM volumes (purple lines) and baseline entorhinal cortex volumes (blue lines). The *y*-axes reflect APC in the entorhinal cortex (purple lines) and in the NbM (blue lines). Baseline volumes and APC units were *z*-scored (z). BL = baseline volume; nCSF = normal CSF group. $^{***}P < 0.001$; $^{*}P < 0.01$; $^{*}P < 0.05$.

$P = 0.12$, CI: –0.03 to 0.27; Fig. 3J] (Supplementary Table 2). Nor was there a significant interaction between CSF group and the relationship between entorhinal cortex and NbM in the pooled sample [$t(826) = 1$, $P = 0.62$; Fig. 3J].

We then directly compared the two predictive staging models, NbM→EC and EC→NbM, using a slopes analysis between dependent samples. We found that the coefficients in each model were significantly different from one another in the abnormal CSF group [$z = 5.54$; $P < 0.001$; 95% r CI: 0.1831 to 0.3847] but not in the normal CSF group ($z = 0.08$; $P = 0.931$; 95% r CI: –0.1424 to 0.13) (Fig. 4).

Taken together, our predictive pathological models suggest that neurodegeneration of the cholinergic basal forebrain system may occur in both the abnormal and normal CSF ageing phenotypes, but that abnormal proteopathic pTau/amyloid-β accumulation greatly exacerbates this effect. The results also demonstrate that the EC→NbM model does not fit a neurobiologically plausible predictive staging of neurodegeneration in either the abnormal or normal CSF cohort.

Clinical diagnosis does not moderate the relationship between NbM→EC

Having demonstrated that the NbM→EC relationship was more prominent and reliable in the abnormal CSF group, we then investigated whether the severity of the disease had an impact on the strength of this relationship in the pooled abnormal CSF group. We predicted that the MCI abnormal CSF subgroup would exhibit the strongest pattern of degenerative 'spreading' between NbM and entorhinal cortex, followed by cognitively normal abnormal CSF and Alzheimer's disease abnormal CSF subgroups (Schmitz and Spreng, 2016). Although MCI abnormal CSF individuals exhibited a steeper positive slope compared to the other two diagnostic groups, clinical diagnosis was not a significant moderating effect (Supplementary Fig. 3) [$t(1,479) = 1.65$, $P = 0.49$], indicating that the predictive relationship was robust across clinical diagnostic subgroups of the abnormal CSF cohort.

NbM→EC predictive pathological spreading is anatomically specific

How spatially selective is the observed interrelationship between NbM and entorhinal cortex in the abnormal CSF group? To determine where degeneration is predicted based on NbM integrity, we performed a voxel-wise regression analysis between baseline volumes in the NbM and longitudinal APC in every brain voxel. The model collapsed abnormal CSF individuals across the two ADNI Cohorts into a single 'Pooled' cohort. After FWE correction for multiple comparisons, we found that baseline NbM volumes predicted degeneration in a circumscribed cluster of regions localized to the right entorhinal and perirhinal cortices and in the left middle temporal gyrus (Fig. 5A). The predictive pathological spread of NbM→EC

neurodegeneration therefore exhibits a high degree of anatomical specificity.

In our *a priori* region of interest-based regression models, we found negligible evidence in support of the EC→NbM model. However, following from non-human animal work (de Calignon *et al.*, 2012; Liu *et al.*, 2012; Khan *et al.*, 2014; Wu *et al.*, 2016), we hypothesized that predictive spread of degeneration from entorhinal cortex might target anatomically and functionally connected cortical areas including the parahippocampal and posterior parietal cortices. To test this hypothesis, we computed a second voxel-wise regression analysis in the pooled abnormal CSF group between baseline volumes in the entorhinal cortex and longitudinal APC in every brain voxel of the grey matter mask (refer to the 'Materials and methods' section). After FWE correction, we found that baseline entorhinal cortex volumes predicted longitudinal degeneration in a circumscribed network of temporal cortical regions including the entorhinal, perirhinal, parahippocampal and fusiform cortices and temporal poles (Fig. 5B). Additional clusters were detected in the insular and posterior parietal cortices.

Finally, we tested the same models in the normal CSF cohort, collapsing individuals from both ADNI cohorts. No significant voxels were found at the corrected statistical threshold ($P < 0.05$ FWE) in either of the models (NbM→whole brain; EC→whole brain). Taken together, the voxel-wise regression results show that among individuals expressing abnormal CSF: (i) baseline NbM volumes selectively predict degeneration in the entorhinal cortex and adjacent perirhinal cortex; and (ii) entorhinal cortex degeneration 'spreads' to anatomically and functionally connected areas including the parahippocampal gyrus and other temporoparietal regions (de Calignon *et al.*, 2012; Liu *et al.*, 2012; Khan *et al.*, 2014; Wu *et al.*, 2016).

Discussion

We provide evidence that degeneration in the NbM is an upstream event of subsequent degeneration in the entorhinal cortex and adjacent medial temporal cortices. Our results generalized across two non-overlapping and well-powered datasets. As hypothesized, the NbM→EC relationship was moderated by the presence of abnormal CSF biomarkers of pTau and amyloid-β, consistent with a mechanism of trans-synaptic spread of these proteins across anatomically connected regions. Using whole-brain regression models, we presented novel evidence that the relationship between baseline NbM volumes and neurodegeneration was spatially specific to regions of the entorhinal cortex and the perirhinal cortices. Finally, baseline

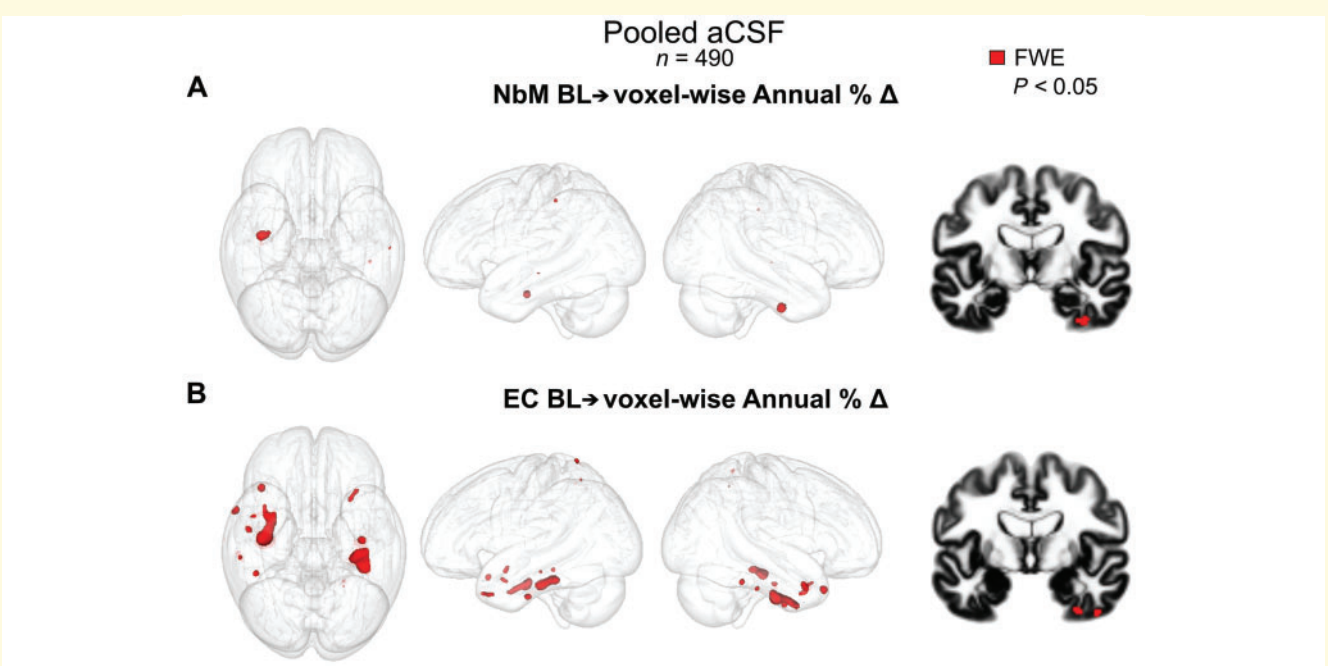

Figure 5 NbM and entorhinal cortex predict distinct patterns of downstream degenerative spreading. Baseline volumes of the NbM and the entorhinal cortex predicting APC in every brain voxel in the pooled abnormal CSF group (aCSF, $n = 490$). In red, voxels showing a significant association with baseline volumes in the NbM (**A**) and in the entorhinal cortex (**B**) with a $P < 0.05$ voxel-level FWE-corrected threshold. Baseline NbM volumes predicted degeneration in the right entorhinal cortex whereas baseline entorhinal cortex volumes predicted degeneration in regions of the temporal and parietal cortices. Results are rendered into an MNI glass brain to the group DARTEL space using Mango (http://ric.uthscsa.edu/mango/). Models were tested for significance using non-parametric permutation testing.

entorhinal cortex volumes predicted neurodegeneration mainly in regions of the temporal cortex, recapitulating neurodegenerative spreading dynamics observed in human *in vivo* structural imaging work (Dickerson *et al*., 2001; Du *et al*., 2001) and mouse models of trans-synaptic tau propagation (de Calignon *et al*., 2012; Liu *et al*., 2012; Khan *et al*., 2014; Wu *et al*., 2016). These findings highlight the importance of the cholinergic basal forebrain nuclei in Alzheimer's disease and motivate novel interventions targeted to these neuronal populations.

The intrinsic properties of the basal forebrain cholinergic neurons, including their morphology and propensity for sustained neuroplasticity throughout adulthood, might be key to understanding why these cell types are selectively vulnerable in Alzheimer's disease (Mesulam, 1999; Mattson and Magnus, 2006; Saxena and Caroni, 2011; Wu *et al*., 2014; Roussarie *et al*., 2019). The NbM cholinergic neurons have large projecting axons with extensive arbours that expand long distances in the CNS (Wu *et al*., 2014; Li *et al*., 2018; Yan *et al*., 2018). Extremely large axons and arbours exert high metabolic demands in order to support their maintenance, repair and transport. A less efficient cellular response to axonal perturbations could increase their vulnerability to the accumulation of abnormal proteins (Wu *et al*., 2014). In addition, large surface areas increase their exposure to toxic environments (Mattson and Magnus, 2006). Consistent with its selective vulnerability, the NbM is one of the most vulnerable regions to the early accumulation of intracellular tau pathology (Mesulam *et al*., 2004; Braak and Del Tredici, 2011, 2015) and intraneuronal amyloid oligomers (Baker-Nigh *et al*., 2015). There is increasing evidence showing that intraneuronal amyloid can have deleterious early effects in neurons, such as disrupting their retrograde axonal transport machinery (Pigino *et al*., 2009), which in turn can cause a neurotrophic deficiency (Bellucci *et al*., 2006) leading to neurodegeneration (De Lacalle *et al*., 1996). Recent functional genomics research examining the molecular profile of different neuronal cell types in the adult brain indicates that those with selective vulnerability to Alzheimer's disease, such as the layer II entorhinal neurons, are selectively enriched for expression of amyloid precursor protein (APP) and microtubule-associated protein tau (MAPT) compared to neurons in primary visual and somatosensory cortices (Roussarie *et al*., 2019). Given the hypothesized physiological roles of APP in synaptic remodelling and MAPT in microtubule formation, increased neuronal expression of these genes might represent a heightened propensity for neuroplasticity in adulthood—consistent with the known role of entorhinal neurons in memory encoding. The cholinergic basal forebrain neurons—which constitute the primary source of acetylcholine for the entire brain—are thought to exhibit a similar propensity for adult neuroplasticity due to their role in learning and memory (Mesulam, 1999). Cholinergic neuromodulation is essential for triggering entorhinal and hippocampal plasticity during encoding of novel sensory information (Sarter *et al*., 2003; Hasselmo, 2006; Botly and De Rosa, 2009; Heys *et al*., 2010; Gu and Yakel, 2011; Mitsushima *et al*., 2013; Schmitz and Duncan, 2018). Whether APP and MAPT expression is similarly elevated in cholinergic basal forebrain remains to be determined. Nevertheless, the cholinergic basal forebrain neurons exhibit a unique mixture of morphological and functional properties which appear to heighten their vulnerability to structural degeneration in the ageing brain.

In this study, the pathological spread of neurodegeneration from the NbM to the entorhinal cortex was exacerbated in individuals with abnormal levels of CSF pTau and amyloid-β. Evidence from non-human animal studies shows that protein aggregates can spread trans-synaptically to neuroanatomically connected regions. In an APP mouse model of Alzheimer's disease, neuronal accumulation of amyloid-β was observed first in the entorhinal cortex, followed by the dentate gyrus, a downstream region receiving monosynaptic projections from the entorhinal cortex (Harris *et al*., 2010). Evidence further suggests that tau aggregates propagate from the entorhinal cortex to limbic and then neocortical connected areas (de Calignon *et al*., 2012; Liu *et al*., 2012; Walker *et al*., 2013; Khan *et al*., 2014; Wu *et al*., 2016). For example, in mice that expressed human tau restricted to the entorhinal cortex, the axonal terminals of the entorhinal cortex projecting neurons showed increasing markers of tauopathy over time (Liu *et al*., 2012). In all, this shows that amyloid-β and pTau can propagate synaptically across neural networks of anatomically connected vulnerable cells. If the NbM is one of the earliest regions to accumulate tau and amyloid-β, then these proteins may spread to the entorhinal cortex trans-synaptically, inducing the observed downstream neurodegeneration. Our results are therefore compatible with animal research showing a trans-synaptic mechanism of abnormal spreading of tau proteins. However, to ultimately demonstrate that degeneration in the entorhinal cortex is driven by the spread of tau pathology from the NbM in humans, longitudinal studies integrating both structural MRI and tau PET are needed. In addition, we observed a relationship between the NbM→EC in the normal CSF group. This effect was weaker and not reliable across samples, indicating the possibility that there are other age-related pressures on the NbM cholinergic neurons independent from amyloid-β and pTau (Wurtman *et al*., 1990; Nitsch *et al*., 1992; Wurtman, 1992). Nevertheless, we found that the presence of abnormal amyloid-β and pTau was the strongest moderating factor on the relationship between NbM→EC; this relationship was robust to differences in *APOE* genotype, clinical diagnosis and ADNI cohort (magnetic resonance field strength). Collectively, our findings indicate that degeneration of the NbM and entorhinal cortex pathway is likely influenced by multiple genetic and environmental risk factors which may disrupt amyloid and tau proteostasis in the ageing brain, such as vascular health (Iturria-Medina *et al*., 2016). Additional modelling of these complex multivariate changes

will be necessary to unravel the age-related factors that most reliably predict abnormal accumulation of amyloid and tau.

Our study extends on prior *in vivo* structural MRI studies demonstrating pronounced basal forebrain degeneration in the context of ageing and Alzheimer's disease. For instance, in prior work, reduced basal forebrain volumes have been observed in MCI patients both cross-sectionally (Teipel *et al.*, 2005, 2011, 2017; Grothe *et al.*, 2010, 2012; Kilimann *et al.*, 2014, 2017; Cantero *et al.*, 2017) and longitudinally (Grothe *et al.*, 2013; Schmitz and Spreng, 2016; Cavedo *et al.*, 2017; Schmitz *et al.*, 2018). Here we used a novel combination of CSF biomarkers, longitudinal structural MRI, a large replication sample and regression-based whole-brain modelling to demonstrate a reliable (Fig. 3A–E) and highly specific (Fig. 5A) sequence of neurodegeneration from the NbM to the entorhinal cortex. Our evidence in favour of the NbM→EC model accords with numerous post-mortem histology studies implicating the selective vulnerability of NbM cholinergic cell populations (Davies and Maloney, 1976; Whitehouse *et al.*, 1981; Arendt *et al.*, 1985, 2015; Mesulam *et al.*, 2004; Geula *et al.*, 2008; Braak and Del Tredici, 2011, 2015; Braak *et al.*, 2011; Baker-Nigh *et al.*, 2015; Hanna Al-Shaikh *et al.*, 2019). However, predictive staging based on histological strategies are limited by the heterogeneity of the post-mortem samples, the inability to track pathology with progressive neurodegeneration within individuals, the variability in tissue staining techniques used to profile underlying pathology, and the variability in anatomical coverage across both cortical and subcortical regions. We overcame these limitations by using an *in vivo* longitudinal neuroimaging strategy of predictive pathological staging in a large cohort of >800 older adults. We quantified the baseline CSF profile of amyloid-β and pTau in each individual based on the automated Elecsys® protocol, which was harmonized between samples. We then applied an independently defined cut-off point to delineate unbiased groups of individuals exhibiting abnormal and normal CSF biomarkers. By comparing the spreading dynamics of neurodegeneration between these two groups, we demonstrated that baseline NbM volumes predicted an accelerated annual rate of degeneration in a future time point in the entorhinal cortex. Although this effect was strongest in the right hemisphere entorhinal cortex, additional predictive effects in the left hemisphere entorhinal cortex were detectable at a more liberal uncorrected threshold. It is currently unknown whether hemispheric asymmetries exist in the vulnerability of the NbM→EC pathway, nor what risk factors would influence such asymmetry. Finally, we found evidence that this neuropathological background was associated with neurodegenerative spreading from entorhinal cortex to targets of its projections in the medial temporal lobes. These latter findings parallel those of recent cross-species translational research comparing transgenic mouse models of Alzheimer's disease with at-risk human participants (Khan *et al.*, 2014). In all, our results demonstrate that NbM degeneration is an earlier pathological event in the Alzheimer's disease pathological cascade.

Although support for the NbM→EC model reliably generalized between two different populations, we cannot infer from this finding whether the NbM is the origin of Alzheimer's disease pathophysiology. Based on post-mortem histological analyses, other ascending neuromodulatory cell populations have been found to exhibit early degeneration in ageing, MCI and Alzheimer's disease. In particular, post-mortem histology work has repeatedly identified severe tau accumulation and neuronal cell loss in the cluster of noradrenergic brainstem neurons known as the locus coeruleus (Zarow *et al.*, 2003; Heneka *et al.*, 2006, 2010; Grudzien *et al.*, 2007; Braak and Del Tredici, 2011, 2015; Braak *et al.*, 2011; Arendt *et al.*, 2015; Ghosh *et al.*, 2019). Like neurons of the cholinergic basal forebrain and layer II entorhinal cortex, the locus coeruleus norandrenergic neurons have large complex axonal projections (Schwarz and Luo, 2015; Schwarz *et al.*, 2015), which may account in part for their apparent selective vulnerability to early degeneration. The T_1-weighted structural MRI data used in this study are poorly optimized for quantifying grey matter volume in brainstem nuclei such as the locus coeruleus (Lambert *et al.*, 2013*a*, *b*). Nevertheless, stereotactic probabilistic atlases of the human locus coeruleus are available (Keren *et al.*, 2009; Tona *et al.*, 2017) and novel magnetic resonance sequences optimized for quantifying the brainstem volume *in vivo* are under development (Lambert *et al.*, 2013*a*, *b*). Future work examining anatomically comprehensive staging models of Alzheimer's disease pathophysiology would therefore benefit by integrating these magnetic resonance sequences into their scan acquisition protocols.

To understand the predictive staging of basal forebrain neurodegeneration at even earlier stages of Alzheimer's disease, another necessary step will involve parallel *in vivo* quantification of longitudinal changes in both the grey and white matter microstructure. Diffusion-weighted MRI techniques enable tractography-based analysis of the basal forebrain white matter projections (Kerbler *et al.*, 2013; Ray *et al.*, 2015). PET, combined with radiotracers that selectively bind to the vesicular acetylcholine transporter (VAChT), a glycoprotein located on presynaptic cholinergic terminals, represents another promising tool for quantifying the integrity of the cholinergic basal forebrain projectome *in vivo* (Aghourian *et al.*, 2017; Schmitz *et al.*, 2018). Because degeneration of the cholinergic cell body in the NbM is likely preceded by a period of distal axonal degeneration (Yan *et al.*, 2018), these neuroimaging techniques might provide insight into even earlier stages of Alzheimer's disease pathophysiology. For instance, spatially selective genetic knock-down of VAChT in the mouse hippocampus was found to alter RNA metabolism and induce Alzheimer's disease-like changes in proteostasis (Kolisnyk *et al.*, 2016), suggesting that loss of cortical cholinergic input is by itself sufficient to induce pathophysiology. Whether age-related cortical cholinergic denervation

induces similar pathophysiology in the human brain remains to be determined.

Finally, we note that because ADNI is a multi-site study, MRI data were acquired in multiple different scanners, which might introduce variability in the quality of the images used to quantify grey matter volume. Despite significant efforts to harmonize the acquisition and postprocessing phases of neuroimaging data (Jack *et al.*, 2008), non-biological variations between scanners may impact the volumetric estimations from T_1 images (Jovicich *et al.*, 2009; Kruggel *et al.*, 2010). However, studies using structural MRI to examine Alzheimer's disease neurodegeneration do not show an interaction between scanner and diagnosis and a smaller effect of scanner than of diagnostic group in grey matter regions (Stonnington *et al.*, 2008). In the present study, we calculated annualized per cent rates to evaluate grey matter changes over time. Presumably, calculating a difference between successive time points would minimize the influence of variation in global intensity caused by interscanner differences. In addition, our main regression results (Fig. 3E and J) were robust to the inclusion of the different sites (scanners) as a fixed-effect covariate and the distribution of abnormal and normal CSF participants was comparable across sites (data not shown). Although it is challenging to perfectly systematize large multicentre studies, we believe efforts such as ADNI are currently the best resources available for *in vivo* staging of Alzheimer's disease progression.

In conclusion, the current study provides reliable and anatomically specific support for a predictive pathological staging model of Alzheimer's disease that progresses in the following sequence: NbM→EC→Neocortex. In all, our findings call into question a prevailing view of Alzheimer's disease pathogenesis, suggesting instead that degeneration of the basal forebrain cholinergic projection system is an upstream event to that of its most vulnerable cortical targets in the entorhinal cortex. If the cholinergic neurons of the basal forebrain are selectively vulnerable to the early accumulation and propagation of Alzheimer's disease pathology, then interventions targeting these neuronal populations in early disease stages may be useful for modifying disease progression prior to cognitive decline.

Funding

Data collection and sharing for this project was funded by the Alzheimer's Disease Neuroimaging Initiative (ADNI) (National Institutes of Health Grant U01 AG024904) and DOD ADNI (Department of Defense award number W81XWH-12-2-0012). ADNI is funded by the National Institute on Aging, the National Institute of Biomedical Imaging and Bioengineering, and through generous contributions from the following: AbbVie, Alzheimer's Association; Alzheimer's Drug Discovery Foundation; Araclon Biotech; BioClinica, Inc.; Biogen; Bristol-Myers Squibb Company; CereSpir, Inc.; Cogstate; Eisai Inc.; Elan Pharmaceuticals, Inc.; Eli Lilly and Company; EuroImmun; F. Hoffmann-La Roche Ltd and its affiliated company Genentech, Inc.; Fujirebio; GE Healthcare; IXICO Ltd.; Janssen Alzheimer Immunotherapy Research & Development, LLC.; Johnson & Johnson Pharmaceutical Research & Development LLC.; Lumosity; Lundbeck; Merck & Co., Inc.; Meso Scale Diagnostics, LLC.; NeuroRx Research; Neurotrack Technologies; Novartis Pharmaceuticals Corporation; Pfizer Inc.; Piramal Imaging; Servier; Takeda Pharmaceutical Company; and Transition Therapeutics. The Canadian Institutes of Health Research is providing funds to support ADNI clinical sites in Canada. Private sector contributions are facilitated by the Foundation for the National Institutes of Health (www.fnih.org). The grantee organization is the Northern California Institute for Research and Education, and the study is coordinated by the Alzheimer's Therapeutic Research Institute at the University of Southern California. ADNI data are disseminated by the Laboratory for Neuro Imaging at the University of Southern California. This work was supported in part by a grant from the NIA (R03 RAG060263A) (T.W.S. and R.N.S.) and the Canada First Research Excellence Fund (T.W.S. and R.N.S.). S.F.C was supported by the Doctoral College "Imaging the Mind" (FWF-W1233) of the Austrian Science Fund. We thank Didac Vidal-Piñeiro and the LCBC group in Oslo for feedback on this manuscript. This work was supported in part by a Pfizer Scientific Services Evaluation Agreement to R.N.S.

Competing interests

K.R.A.V.D. and J.A.G. are currently employed by Pfizer.

Supplementary material

Supplementary material is available at *Brain* online.

References

Aghourian M, Legault-Denis C, SoucyJP, Rosa-NetoP, Gauthier S, Kostikov A, et al. Quantification of brain cholinergic denervation in Alzheimer's disease using PET imaging with [18F]-FEOBV. Mol Psychiatry 2017; 11: 1531–8.

Aisen PS, Petersen RC, Donohue M, Weiner MW. Alzheimer's disease neuroimaging I. Alzheimer's disease neuroimaging initiative 2 clinical core: progress and plans. Alzheimers Dement 2015; 11: 734–9.

Aisen PS, Petersen RC, Donohue MC, Gamst A, Raman R, Thomas RG, et al. Clinical core of the Alzheimer's disease neuroimaging initiative: progress and plans. Alzheimers Dement 2010; 6: 239–46.

Amunts K, Kedo O, Kindler M, Pieperhoff P, Mohlberg H, Shah NJ, et al. Cytoarchitectonic mapping of the human amygdala, hippocampal region and entorhinal cortex: intersubject variability and probability maps. Anat Embryol (Berl) 2005; 210: 343–52.

Arendt T, Bigl V, Tennstedt A, Arendt A. Neuronal loss in different parts of the nucleus basalis is related to neuritic plaque formation in

cortical target areas in Alzheimer's disease. Neuroscience 1985; 14: 1–14.
Arendt T, Bruckner MK, Morawski M, Jager C, Gertz HJ. Early neurone loss in Alzheimer's disease: cortical or subcortical? Acta Neuropathol Commun 2015; 3: 10.
Ashburner J. A fast diffeomorphic image registration algorithm. Neuroimage 2007; 38: 95–113.
Ashburner J, Ridgway GR. Symmetric diffeomorphic modeling of longitudinal structural MRI. Front Neurosci 2012; 6: 197.
Baker-Nigh A, Vahedi S, Davis EG, Weintraub S, Bigio EH, Klein WL, et al. Neuronal amyloid-beta accumulation within cholinergic basal forebrain in ageing and Alzheimer's disease. Brain 2015; 138: 1722–37.
Bellucci A, Luccarini I, Scali C, Prosperi C, Giovannini MG, Pepeu G, et al. Cholinergic dysfunction, neuronal damage and axonal loss in TgCRND8 mice. Neurobiol Dis 2006; 23: 260–72.
Botly LC, De Rosa E. Cholinergic deafferentation of the neocortex using 192 IgG-saporin impairs feature binding in rats. J Neurosci 2009; 29: 4120–30.
Braak H, Del Tredici K. The pathological process underlying Alzheimer's disease in individuals under thirty. Acta Neuropathol 2011; 121: 171–81.
Braak H, Del Tredici K. The preclinical phase of the pathological process underlying sporadic Alzheimer's disease. Brain 2015; 138: 2814–33.
Braak H, Thal DR, Ghebremedhin E, Del Tredici K. Stages of the pathologic process in Alzheimer disease: age categories from 1 to 100 years. J Neuropathol Exp Neurol 2011; 70: 960–9.
Cantero JL, Zaborszky L, Atienza M. Volume loss of the nucleus basalis of meynert is associated with atrophy of innervated regions in mild cognitive impairment. Cereb Cortex 2017; 27: 3881–9.
Cavedo E, Grothe MJ, Colliot O, Lista S, Chupin M, Dormont D, et al. Reduced basal forebrain atrophy progression in a randomized Donepezil trial in prodromal Alzheimer's disease. Sci Rep 2017; 7: 11706.
Corder EH, Saunders AM, Strittmatter WJ, Schmechel DE, Gaskell PC, Small GW, et al. Gene dose of apolipoprotein E type 4 allele and the risk of Alzheimer's disease in late onset families. Science 1993; 261: 921–3.
Crane PK, Carle A, Gibbons LE, Insel P, Mackin RS, Gross A, et al. Development and assessment of a composite score for memory in the Alzheimer's disease neuroimaging initiative (ADNI). Brain Imaging Behav 2012; 6: 502–16.
Davies P, Maloney AJ. Selective loss of central cholinergic neurons in Alzheimer's disease. Lancet 1976; 2: 1403.
de Calignon A, Polydoro M, Suarez-Calvet M, William C, Adamowicz DH, Kopeikina KJ, et al. Propagation of tau pathology in a model of early Alzheimer's disease. Neuron 2012; 73: 685–97.
De Lacalle S, Cooper JD, Svendsen CN, Dunnett SB, Sofroniew MV. Reduced retrograde labelling with fluorescent tracer accompanies neuronal atrophy of basal forebrain cholinergic neurons in aged rats. Neuroscience 1996; 75: 19–27.
de Toledo-Morrell L, Goncharova I, Dickerson B, Wilson RS, Bennett DA. From healthy aging to early Alzheimer's disease: in vivo detection of entorhinal cortex atrophy. Ann N Y Acad Sci 2000; 911: 240–53.
de Toledo-Morrell L, Stoub TR, Bulgakova M, Wilson RS, Bennett DA, Leurgans S, et al. MRI-derived entorhinal volume is a good predictor of conversion from MCI to AD. Neurobiol Aging 2004; 25: 1197–203.
Dickerson BC, Goncharova I, Sullivan MP, Forchetti C, Wilson RS, Bennett DA, et al. MRI-derived entorhinal and hippocampal atrophy in incipient and very mild Alzheimer's disease. Neurobiol Aging 2001; 22: 747–54.
Diedenhofen B, Musch J. cocor: a comprehensive solution for the statistical comparison of correlations. PLoS One 2015; 10: e0121945.
Du AT, Schuff N, Amend D, Laakso MP, Hsu YY, Jagust WJ, et al. Magnetic resonance imaging of the entorhinal cortex and hippocampus in mild cognitive impairment and Alzheimer's disease. J Neurol Neurosurg Psychiatry 2001; 71: 441–7.
Farrer LA, Cupples LA, Haines JL, Hyman B, Kukull WA, Mayeux R, et al. Effects of age, sex, and ethnicity on the association between apolipoprotein E genotype and Alzheimer disease. A meta-analysis. APOE and Alzheimer Disease Meta Analysis Consortium. JAMA 1997; 278: 1349–56.
Frisoni GB, Fox NC, Jack CR Jr, Scheltens P, Thompson PM. The clinical use of structural MRI in Alzheimer disease. Nat Rev Neurol 2010; 6: 67–77.
Gerardin E, Chetelat G, Chupin M, Cuingnet R, Desgranges B, Kim HS, et al. Multidimensional classification of hippocampal shape features discriminates Alzheimer's disease and mild cognitive impairment from normal aging. Neuroimage 2009; 47: 1476–86.
Geula C, Nagykery N, Nicholas A, Wu CK. Cholinergic neuronal and axonal abnormalities are present early in aging and in Alzheimer disease. J Neuropathol Exp Neurol 2008; 67: 309–18.
Ghosh A, Torraville SE, Mukherjee B, Walling SG, Martin GM, Harley CW, et al. An experimental model of Braak's pretangle proposal for the origin of Alzheimer's disease: the role of locus coeruleus in early symptom development. Alzheimers Res Ther 2019; 11: 59.
Gibbons LE, Carle AC, Mackin RS, Harvey D, Mukherjee S, Insel P, et al. A composite score for executive functioning, validated in Alzheimer's Disease Neuroimaging Initiative (ADNI) participants with baseline mild cognitive impairment. Brain Imaging Behav 2012; 6: 517–27.
Good CD, Scahill RI, Fox NC, Ashburner J, Friston KJ, Chan D, et al. Automatic differentiation of anatomical patterns in the human brain: validation with studies of degenerative dementias. Neuroimage 2002; 17: 29–46.
Grothe M, Heinsen H, Teipel S. Longitudinal measures of cholinergic forebrain atrophy in the transition from healthy aging to Alzheimer's disease. Neurobiol Aging 2013; 34: 1210–20.
Grothe M, Heinsen H, Teipel SJ. Atrophy of the cholinergic Basal forebrain over the adult age range and in early stages of Alzheimer's disease. Biol Psychiatry 2012; 71: 805–13.
Grothe MJ, Sepulcre J, Gonzalez-Escamilla G, Jelistratova I, Scholl M, Hansson O, et al. Molecular properties underlying regional vulnerability to Alzheimer's disease pathology. Brain 2018; 141: 2755–71.
Grothe M, Zaborszky L, Atienza M, Gil-Neciga E, Rodriguez-Romero R, Teipel SJ, et al. Reduction of basal forebrain cholinergic system parallels cognitive impairment in patients at high risk of developing Alzheimer's disease. Cereb Cortex 2010; 20: 1685–95.
Grudzien A, Shaw P, Weintraub S, Bigio E, Mash DC, Mesulam MM. Locus coeruleus neurofibrillary degeneration in aging, mild cognitive impairment and early Alzheimer's disease. Neurobiol Aging 2007; 28: 327–35.
Gu Z, Yakel JL. Timing-dependent septal cholinergic induction of dynamic hippocampal synaptic plasticity. Neuron 2011; 71: 155–65.
Hanna Al-Shaikh FS, Duara R, Crook JE, Lesser ER, Schaeverbeke J, Hinkle KM, et al. Selective vulnerability of the nucleus basalis of Meynert among neuropathologic subtypes of Alzheimer disease. JAMA Neurol 2019. doi: 10.1001/jamaneurol.2019.3606.
Hanseeuw BJ, Betensky RA, Jacobs HIL, Schultz AP, Sepulcre J, Becker JA, et al. Association of amyloid and tau with cognition in preclinical Alzheimer disease: a longitudinal study. JAMA Neurol 2019. doi: 10.1001/jamaneurol.2019.1424.
Hansson O, Seibyl J, Stomrud E, Zetterberg H, Trojanowski JQ, Bittner T, et al. CSF biomarkers of Alzheimer's disease concord with amyloid-beta PET and predict clinical progression: a study of fully automated immunoassays in BioFINDER and ADNI cohorts. Alzheimers Dement 2018; 14: 1470–81.
Harris JA, Devidze N, Verret L, Ho K, Halabisky B, Thwin MT, et al. Transsynaptic progression of amyloid-beta-induced neuronal dysfunction within the entorhinal-hippocampal network. Neuron 2010; 68: 428–41.

Harrison TM, La Joie R, Maass A, Baker SL, Swinnerton K, Fenton L, et al. Longitudinal tau accumulation and atrophy in aging and Alzheimer disease. Ann Neurol 2019; 85: 229–40.

Hasselmo ME. The role of acetylcholine in learning and memory. Curr Opin Neurobiol 2006; 16: 710–5.

Hayes AF. Introduction to mediation, moderation, and conditional process analysis: a regression-based approach. 2nd edn. New York, NY: The Guilford Press; 2017.

Heneka MT, Nadrigny F, Regen T, Martinez-Hernandez A, Dumitrescu-Ozimek L, Terwel D, et al. Locus ceruleus controls Alzheimer's disease pathology by modulating microglial functions through norepinephrine. Proc Natl Acad Sci U S A 2010; 107: 6058–63.

Heneka MT, Ramanathan M, Jacobs AH, Dumitrescu-Ozimek L, Bilkei-Gorzo A, Debeir T, et al. Locus ceruleus degeneration promotes Alzheimer pathogenesis in amyloid precursor protein 23 transgenic mice. J Neurosci 2006; 26: 1343–54.

Hett K, Ta VT, Catheline G, Tourdias T, Manjon JV, Coupe P, et al. Multimodal hippocampal subfield grading for Alzheimer's disease classification. Sci Rep 2019; 9: 13845.

Heys JG, Giocomo LM, Hasselmo ME. Cholinergic modulation of the resonance properties of stellate cells in layer II of medial entorhinal cortex. J Neurophysiol 2010; 104: 258–70.

Hirata Y, Matsuda H, Nemoto K, Ohnishi T, Hirao K, Yamashita F, et al. Voxel-based morphometry to discriminate early Alzheimer's disease from controls. Neurosci Lett 2005; 382: 269–74.

Iturria-Medina Y, Sotero RC, Toussaint PJ, Mateos-Perez JM, Evans AC. Early role of vascular dysregulation on late-onset Alzheimer's disease based on multifactorial data-driven analysis. Nat Commun 2016; 7: 11934.

Jack CR Jr, Bernstein MA, Fox NC, Thompson P, Alexander G, Harvey D, et al. The Alzheimer's disease neuroimaging initiative (ADNI): MRI methods. J Magn Reson Imaging 2008; 27: 685–91.

Jack CR Jr, Knopman DS, Jagust WJ, Petersen RC, Weiner MW, Aisen PS, et al. Tracking pathophysiological processes in Alzheimer's disease: an updated hypothetical model of dynamic biomarkers. Lancet Neurol 2013; 12: 207–16.

Jovicich J, Czanner S, Han X, Salat D, van der Kouwe A, Quinn B, et al. MRI-derived measurements of human subcortical, ventricular and intracranial brain volumes: reliability effects of scan sessions, acquisition sequences, data analyses, scanner upgrade, scanner vendors and field strengths. Neuroimage 2009; 46: 177–92.

Karas GB, Scheltens P, Rombouts SA, Visser PJ, van Schijndel RA, Fox NC, et al. Global and local gray matter loss in mild cognitive impairment and Alzheimer's disease. Neuroimage 2004; 23: 708–16.

Kerbler GM, Hamlin AS, Pannek K, Kurniawan ND, Keller MD, Rose SE, et al. Diffusion-weighted magnetic resonance imaging detection of basal forebrain cholinergic degeneration in a mouse model. Neuroimage 2013; 66: 133–41.

Keren NI, Lozar CT, Harris KC, Morgan PS, Eckert MA. In vivo mapping of the human locus coeruleus. Neuroimage 2009; 47: 1261–7.

Khan UA, Liu L, Provenzano FA, Berman DE, Profaci CP, Sloan R, et al. Molecular drivers and cortical spread of lateral entorhinal cortex dysfunction in preclinical Alzheimer's disease. Nat Neurosci 2014; 17: 304–11.

Kilimann I, Grothe M, Heinsen H, Alho EJ, Grinberg L, Amaro E Jr, et al. Subregional basal forebrain atrophy in Alzheimer's disease: a multicenter study. J Alzheimer's Dis 2014; 40: 687–700.

Kilimann I, Hausner L, Fellgiebel A, Filippi M, Wurdemann TJ, Heinsen H, et al. Parallel atrophy of cortex and basal forebrain cholinergic system in mild cognitive impairment. Cereb Cortex 2017; 27: 1841–8.

Kloppel S, Stonnington CM, Chu C, Draganski B, Scahill RI, Rohrer JD, et al. Automatic classification of MR scans in Alzheimer's disease. Brain 2008; 131: 681–9.

Kolisnyk B, Al-Onaizi M, Soreq L, Barbash S, Bekenstein U, Haberman N, et al. Cholinergic surveillance over hippocampal RNA metabolism and Alzheimer's-like pathology. Cereb Cortex 2016; 36: 6287–96.

Kruggel F, Turner J, Muftuler LT. Alzheimer's Disease Neuroimaging I. Impact of scanner hardware and imaging protocol on image quality and compartment volume precision in the ADNI cohort. Neuroimage 2010; 49: 2123–33.

Lambert C, Chowdhury R, Fitzgerald TH, Fleming SM, Lutti A, Hutton C, et al. Characterizing aging in the human brainstem using quantitative multimodal MRI analysis. Front Hum Neurosci 2013a; 7: 462.

Lambert C, Lutti A, Helms G, Frackowiak R, Ashburner J. Multiparametric brainstem segmentation using a modified multivariate mixture of Gaussians. Neuroimage Clin 2013b; 2: 684–94.

Li X, Yu B, Sun Q, Zhang Y, Ren M, Zhang X, et al. Generation of a whole-brain atlas for the cholinergic system and mesoscopic projectome analysis of basal forebrain cholinergic neurons. Proc Natl Acad Sci U S A 2018; 115: 415–20.

Liu L, Drouet V, Wu JW, Witter MP, Small SA, Clelland C, et al. Trans-synaptic spread of tau pathology in vivo. PLoS One 2012; 7: e31302.

Ma D, Popuri K, Bhalla M, Sangha O, Lu D, Cao J, et al. Quantitative assessment of field strength, total intracranial volume, sex, and age effects on the goodness of harmonization for volumetric analysis on the ADNI database. Hum Brain Mapp 2019; 40: 1507–27.

Malone IB, Leung KK, Clegg S, Barnes J, Whitwell JL, Ashburner J, et al. Accurate automatic estimation of total intracranial volume: a nuisance variable with less nuisance. Neuroimage 2015; 104: 366–72.

Mattson MP, Magnus T. Ageing and neuronal vulnerability. Nat Rev Neurosci 2006; 7: 278–94.

Mechelli A, Price CJ, Friston KJ, Ashburner J. Voxel-based morphometry of the human brain: methods and applications. Curr Med Imaging Rev 2005; 1: 1–10.

Mesulam M, Shaw P, Mash D, Weintraub S. Cholinergic nucleus basalis tauopathy emerges early in the aging-MCI-AD continuum. Ann Neurol 2004; 55: 815–28.

Mesulam MM. Neuroplasticity failure in Alzheimer's disease: bridging the gap between plaques and tangles. Neuron 1999; 24: 521–9.

Mesulam MM, Geula C. Nucleus basalis (Ch4) and cortical cholinergic innervation in the human brain: observations based on the distribution of acetylcholinesterase and choline acetyltransferase. J Comp Neurol 1988; 275: 216–40.

Mesulam MM, Mufson EJ, Levey AI, Wainer BH. Cholinergic innervation of cortex by the basal forebrain: cytochemistry and cortical connections of the septal area, diagonal band nuclei, nucleus basalis (substantia innominata), and hypothalamus in the rhesus monkey. J Comp Neurol 1983a; 214: 170–97.

Mesulam MM, Mufson EJ, Wainer BH, Levey AI. Central cholinergic pathways in the rat: an overview based on an alternative nomenclature (Ch1-Ch6). Neuroscience 1983b; 10: 1185–201.

Mitsushima D, Sano A, Takahashi T. A cholinergic trigger drives learning-induced plasticity at hippocampal synapses. Nat Commun 2013; 4: 2760.

Mueller SG, Weiner MW, Thal LJ, Petersen RC, Jack CR, Jagust W, et al. Ways toward an early diagnosis in Alzheimer's disease: the Alzheimer's Disease Neuroimaging Initiative (ADNI). Alzheimers Dement 2005; 1: 55–66.

Nichols TE, Holmes AP. Nonparametric permutation tests for functional neuroimaging: a primer with examples. Hum Brain Mapp 2002; 15: 1–25.

Nitsch RM, Blusztajn JK, Pittas AG, Slack BE, Growdon JH, Wurtman RJ. Evidence for a membrane defect in Alzheimer disease brain. Proc Natl Acad Sci U S A 1992; 89: 1671–5.

Petersen RC, Aisen PS, Beckett LA, Donohue MC, Gamst AC, Harvey DJ, et al. Alzheimer's Disease Neuroimaging Initiative (ADNI): clinical characterization. Neurology 2010; 74: 201–9.

Pigino G, Morfini G, Atagi Y, Deshpande A, Yu C, Jungbauer L, et al. Disruption of fast axonal transport is a pathogenic mechanism for intraneuronal amyloid beta. Proc Natl Acad Sci U S A 2009; 106: 5907–12.

Poirier J. Apolipoprotein E in animal models of CNS injury and in Alzheimer's disease. Trends Neurosci 1994; 17: 525–30.

Poirier J, Davignon J, Bouthillier D, Kogan S, Bertrand P, Gauthier S. Apolipoprotein E polymorphism and Alzheimer's disease. Lancet 1993; 342: 697–9.

Poirier J, Delisle MC, Quirion R, Aubert I, Farlow M, Lahiri D, et al. Apolipoprotein E4 allele as a predictor of cholinergic deficits and treatment outcome in Alzheimer disease. Proc Natl Acad Sci U S A 1995; 92: 12260–4.

Ray NJ, Metzler-Baddeley C, Khondoker MR, Grothe MJ, Teipel S, Wright P, et al. Cholinergic basal forebrain structure influences the reconfiguration of white matter connections to support residual memory in mild cognitive impairment. J Neurosci 2015; 35: 739–47.

Roussarie JP, Yao V, Plautz Z, Kasturia S, Albornoz C, Schmidt EF, et al. Selective neuronal vulnerability in Alzheimer's disease: a network-based analysis. bioRxiv 2019. doi: 10.1101/499897.

Sarter M, Bruno JP, Givens B. Attentional functions of cortical cholinergic inputs: what does it mean for learning and memory? Neurobiol Learn Mem 2003; 80: 245–56.

Saxena S, Caroni P. Selective neuronal vulnerability in neurodegenerative diseases: from stressor thresholds to degeneration. Neuron 2011; 71: 35–48.

Saykin AJ, Shen L, Foroud TM, Potkin SG, Swaminathan S, Kim S, et al. Alzheimer's disease neuroimaging initiative biomarkers as quantitative phenotypes: genetics core aims, progress, and plans. Alzheimers Dement 2010; 6: 265–73.

Schindler SE, Gray JD, Gordon BA, Xiong C, Batrla-Utermann R, Quan M, et al. Cerebrospinal fluid biomarkers measured by Elecsys assays compared to amyloid imaging. Alzheimers Dement 2018; 14: 1460–9.

Schmitz TW, Duncan J. Normalization and the cholinergic microcircuit: a unified basis for attention. Trends Cogn Sci 2018; 22: 422–37.

Schmitz TW, Mur M, Aghourian M, Bedard MA, Spreng RN. Alzheimer's disease neuroimaging I. Longitudinal Alzheimer's degeneration reflects the spatial topography of cholinergic basal forebrain projections. Cell Rep 2018; 24: 38–46.

Schmitz TW, Spreng RN. Basal forebrain degeneration precedes and predicts the cortical spread of Alzheimer's pathology. Nat Commun 2016; 7: 13249.

Schwarz LA, Luo L. Organization of the locus coeruleus-norepinephrine system. Curr Biol 2015; 25: R1051.

Schwarz LA, Miyamichi K, Gao XJ, Beier KT, Weissbourd B, DeLoach KE, et al. Viral-genetic tracing of the input-output organization of a central noradrenaline circuit. Nature 2015; 524: 88–92.

Sepulcre J, Grothe MJ, d'Oleire Uquillas F, Ortiz-Teran L, Diez I, Yang HS, et al. Neurogenetic contributions to amyloid beta and tau spreading in the human cortex. Nat Med 2018; 24: 1910–8.

Shaw LM, Vanderstichele H, Knapik-Czajka M, Clark CM, Aisen PS, Petersen RC, et al. Cerebrospinal fluid biomarker signature in Alzheimer's disease neuroimaging initiative subjects. Ann Neurol 2009; 65: 403–13.

Sorensen L, Igel C, Liv Hansen N, Osler M, Lauritzen M, Rostrup E, et al. Early detection of Alzheimer's disease using MRI hippocampal texture. Hum Brain Mapp 2016; 37: 1148–61.

Stonnington CM, Tan G, Kloppel S, Chu C, Draganski B, Jack CR Jr, et al. Interpreting scan data acquired from multiple scanners: a study with Alzheimer's disease. Neuroimage 2008; 39: 1180–5.

Strittmatter WJ, Saunders AM, Schmechel D, Pericak-Vance M, Enghild J, Salvesen GS, et al. Apolipoprotein E: high-avidity binding to beta-amyloid and increased frequency of type 4 allele in late-onset familial Alzheimer disease. Proc Natl Acad Sci U S A 1993; 90: 1977–81.

Tamamaki N, Nojyo Y. Projection of the entorhinal layer II neurons in the rat as revealed by intracellular pressure-injection of neurobiotin. Hippocampus 1993; 3: 471–80.

Teipel SJ, Flatz W, Ackl N, Grothe M, Kilimann I, Bokde AL, et al. Brain atrophy in primary progressive aphasia involves the cholinergic basal forebrain and Ayala's nucleus. Psychiatry Res 2014; 221: 187–94.

Teipel SJ, Flatz WH, Heinsen H, Bokde AL, Schoenberg SO, Stockel S, et al. Measurement of basal forebrain atrophy in Alzheimer's disease using MRI. Brain 2005; 128: 2626–44.

Teipel SJ, Keller F, Thyrian JR, Strohmaier U, Altiner A, Hoffmann W, et al. Hippocampus and basal forebrain volumetry for dementia and mild cognitive impairment diagnosis: could it be useful in primary care? J Alzheimer's Dis 2017; 55: 1379–94.

Teipel SJ, Meindl T, Grinberg L, Grothe M, Cantero JL, Reiser MF, et al. The cholinergic system in mild cognitive impairment and Alzheimer's disease: an in vivo MRI and DTI study. Hum Brain Mapp 2011; 32: 1349–62.

Tona KD, Keuken MC, de Rover M, Lakke E, Forstmann BU, Nieuwenhuis S, et al. In vivo visualization of the locus coeruleus in humans: quantifying the test-retest reliability. Brain Struct Funct 2017; 222: 4203–17.

Walker LC, Diamond MI, Duff KE, Hyman BT. Mechanisms of protein seeding in neurodegenerative diseases. JAMA Neurol 2013; 70: 304–10.

Warren JD, Rohrer JD, Schott JM, Fox NC, Hardy J, Rossor MN. Molecular nexopathies: a new paradigm of neurodegenerative disease. Trends Neurosci 2013; 36: 561–9.

Whitehouse PJ, Price DL, Clark AW, Coyle JT, DeLong MR. Alzheimer disease: evidence for selective loss of cholinergic neurons in the nucleus basalis. Ann Neurol 1981; 10: 122–6.

Wu JW, Hussaini SA, Bastille IM, Rodriguez GA, Mrejeru A, Rilett K, et al. Neuronal activity enhances tau propagation and tau pathology in vivo. Nat Neurosci 2016; 19: 1085–92.

Wu H, Williams J, Nathans J. Complete morphologies of basal forebrain cholinergic neurons in the mouse. Elife 2014; 3: e02444.

Wurtman RJ. Choline metabolism as a basis for the selective vulnerability of cholinergic neurons. Trends Neurosci 1992; 15: 117–22.

Wurtman RJ, Blusztajn JK, Ulus IH, Coviella IL, Buyukuysal RL, Growdon JH, et al. Choline metabolism in cholinergic neurons: implications for the pathogenesis of neurodegenerative diseases. Adv Neurol 1990; 51: 117–25.

Wyman BT, Harvey DJ, Crawford K, Bernstein MA, Carmichael O, Cole PE, et al. Standardization of analysis sets for reporting results from ADNI MRI data. Alzheimers Dement 2013; 9: 332–7.

Yan H, Pang P, Chen W, Zhu H, Henok KA, Li H, et al. The lesion analysis of cholinergic neurons in 5XFAD mouse model in the three-dimensional level of whole brain. Mol Neurobiol 2018; 55: 4115–25.

Zaborszky L, Hoemke L, Mohlberg H, Schleicher A, Amunts K, Zilles K. Stereotaxic probabilistic maps of the magnocellular cell groups in human basal forebrain. Neuroimage 2008; 42: 1127–41.

Zarow C, Lyness SA, Mortimer JA, Chui HC. Neuronal loss is greater in the locus coeruleus than nucleus basalis and substantia nigra in Alzheimer and Parkinson diseases. Arch Neurol 2003; 60: 337–41.